J. Fluid Mech. (1985), *vol.* 151, *pp.* 21–53
Printed in Great Britain

On the nature of the entrainment interface of a two-layer fluid subjected to zero-mean-shear turbulence

By HARINDRA J. S. FERNANDO† AND ROBERT R. LONG
Department of Earth and Planetary Sciences, The Johns Hopkins University, Baltimore, MD 21218

(Received 1 August 1983 and in revised form 7 June 1984)

An experimental study was performed to further understanding of turbulent mixing in a two-layer fluid subjected to shear-free turbulence. At low Richardson numbers $Ri\,(=\Delta b D_*^3/K^2$, where Δb is the buoyancy jump, D_* is the depth of a mixed layer and K is 'action') the entrainment seems to occur through the eroding effect of large eddies, whereas at high Ri the large eddies flatten at the density interface and the quasi-isotropic eddies near the interface are responsible for the entrainment. The buoyancy transfer can be well described by a gradient-transport model when the eddy diffusivity is properly defined. At or just above the entrainment interface, the buoyancy flux is of the same order as the dissipation, and the diffusive-flux Richardson number tends to a constant.

The thickness h of the interfacial layer was measured in three different ways and was found to grow linearly with D_* in agreement with preliminary findings of an earlier investigation of Fernando & Long (1983). The buoyancy gradient in the interfacial layer was found to be constant, and the resulting buoyancy conservation law was experimentally verified. The frequency of the interfacial-layer waves appears to vary as $Ri^{\frac{1}{2}}$. The present results, together with the results of the earlier work of Fernando & Long, show a good agreement with a theory of Long (1978*b*) for behaviour at high values of Ri. The closure assumptions of that theory were also verified by our measurements.

1. Introduction

Turbulent mixing in a stably stratified fluid remains a perplexing problem of fluid mechanics. Because of its importance in understanding numerous geophysical phenomena (for example, clear-air turbulence in meteorology and turbulence in the pycnoclines in oceanography) and its large number of technological applications (see e.g. Fisher *et al.* 1979; Fernando 1983), much research effort continues, directed toward a basic understanding of the fundamental aspects of the entrainment process.

Pioneering experiments on turbulent entrainment were performed by Rouse & Dodu (1955), and interest was reawakened and stimulated by Turner (1968), who showed that the entrainment coefficient is a function of Richardson number. Since the work of Turner, a large number of entrainment experiments have been performed, most of which concentrate on the entrainment laws, i.e. the time-dependency of the mixed-layer depth, and the relationship of the entrainment coefficient to the

† Present address: W. M. Keck Laboratory of Hydraulics and Water Resources, California Institute of Technology, Pasadena, CA 91125.

Richardson number. This is a reasonable first approach to the problem and we have made such measurements in an earlier paper (Fernando & Long 1983), but, ultimately, we need to understand the more fundamental aspects of entrainment, for example the mixing mechanism and the nature and the mechanics of the interfacial layer, which appears to play a crucial role. We note also that most of the existing theoretical mixed-layer formulations employ integral balances of momentum, buoyancy and energy, and the resulting equations are solved by conventional closure assumptions. Such theory has proved useful in this and other problems, but it leaves something to be desired in furthering basic understanding.

Specific problems of turbulence in stratified fluids can be very complex, for example the late wake of a submarine moving about in a thermocline, but, even in such applied research, the investigator feels the need for guidance and understanding that can only come from basic research on simpler systems. Measurements of entrainment velocities in stratified-fluid turbulence may be taken to be analogous to measurements of mean velocity in a boundary layer in that both are interesting and obviously needed for many purposes, but more recent research in shear turbulence has stressed the importance of detailed measurements; for example, the relationship of bursting frequencies to outer and inner variables. Similarly, we may argue that we need detailed measurements of the buoyancy flux and dissipation terms in the energy equation to see if they are comparable. Although perception of this need motivates the present study, and to some extent the recent earlier one (Fernando & Long 1983), we acknowledge the priority and importance of still earlier measurements of the properties of grid-generated turbulence in homogeneous and stratified fluids (primarily spectra, r.m.s. velocities and integral lengthscales), by Bouvard & Dumas (1967), Thompson & Turner (1975), Hopfinger & Toly (1976) and McDougall (1979).

Our experiment is with a two-layer stratified-fluid system in which turbulence is created in one layer by a horizontal grid oscillating vertically with small amplitude as shown schematically in figure 1. The choice of this particular experiment was made for many reasons: (i) an oscillating grid is easy to construct and run; (ii) the turbulence it produces may be analogous to certain natural sources, for example wave-breaking in the ocean; (iii) there is a simple energy-source term in the turbulent-energy equation associated with it, namely the energy-flux divergence; (iv) there is a simple theory (Long 1978*a*) that the complicated turbulence production of the grid, related to the oscillation frequency ω, viscosity ν, stroke S and lengths M_1, M_2, ... specifying the geometry, may be parameterized by a single quantity K ('action') having the dimensions of eddy viscosity; (v) measurements of grid turbulence in a homogeneous fluid exist and support this simple theory (Hopfinger & Toly 1976; Dickinson & Long 1978, 1983; McDougall 1979); (vi) there is a rather involved theory (Long 1978*b*) that predicts the behaviour with time and Richardson number of many measurable properties of grid turbulence in linearly stratified and two-layer systems, and this can serve as a guide for our experiment. Moreover, preliminary indications are that this theory makes correct predictions (Folse, Cox & Schexnayder 1981; Fernando & Long 1983); this encourages further testing to increase or lessen our confidence in it. It will be clearly seen that some of the arguments of the theory are generally applicable to stratified-fluid turbulence and this enlarges the scope of possible rewards of such an experimental investigation.

The main purpose of this paper then is to report the continuation of the work appearing in Fernando & Long (1983) on fundamental aspects of the turbulent entrainment process. As mentioned, we were encouraged to pursue this by the excellent agreement between the theoretical solutions of Long (1978*b*) and the

experimental results of Folse *et al.* (1981) and Fernando & Long (1983). The reader will form his own opinion, but we content that our present results add considerable further support to Long's theory.

2. Notation

The paper contains many symbols, because the theory we test is complicated and the experiments we report on cannot be described without introducing new symbols. Therefore we include a list here for the convenience of the reader:

A	constant; $\epsilon = A\sigma_u^3/l$
A_i	constants ($i = 2, \ldots, 5$) depending on the stability of the nonturbulent layer
b	buoyancy
b_i	r.m.s. buoyancy fluctuations (subscripts denote regions R_1, R_2 and R_3)
$\bar{b}_i$	mean buoyancy (subscripts 1, 2, 3 and 23 denote regions R_1, R_2, R_3 and R_2 close to R_3)
$\bar{b}_\infty$	buoyancy of the nonturbulent layer
$\overline{bw}$	buoyancy flux
$B_1, B_2, \ldots$	universal constants
C_2	constant
D_*	depth of the mixed layer measured from a virtual origin
$D_{*\mathrm{f}}$	depth at which large eddies tend to flatten
E	entrainment coefficient
$\mathscr{F}$	energy flux (subscripts correspond to the regions R_1, R_2 and R_3)
g	acceleration due to gravity
h	interfacial-layer thickness (ILT)
h_1	ILT measured by the laser-beam technique
h_2	ILT measured by use of a conductivity probe
h_3	ILT evaluated by use of the buoyancy conservation equation
I	intermittency (subscripts 2, 3, 23 represent regions R_2, R_3 and R_3 close to R_2)
k_s	molecular diffusivity of the stratifying agent
K	'action', defined by observing the mixed-layer deepening in a homogeneous fluid
K_e	eddy diffusivity
K_l	action defined as $K_l = \sigma_u l$
l	integral lengthscale
l_0	Ozmidov lengthscale $(\epsilon_\mathrm{p}/N^3)^{\frac{1}{2}}$
M	mesh size of the grid
$M_1, M_2, \ldots$	lengthscales specifying the grid geometry
N	buoyancy frequency (subscript i denotes the interfacial-layer value)
P	$\frac{1}{2}q_2 + u_\mathrm{e}\Delta b/2\alpha_1$
q	buoyancy flux (subscript denotes regions R_1, R_2 and R_3)
q_d	molecular diffusive buoyancy flux at the entrainment interface
q_T	total buoyancy flux at the entrainment interface
Q	$u_\mathrm{e}\Delta b - q_2$
r	universal constant ($\partial\mathscr{F}/\partial z = r\,\partial u^3/\partial z$)
R_1, R_2, R_3	regions in the stratified system, see figure 1
R_f	local flux Richardson number for stratified shear flow

R_{fd} local diffusive flux Richardson number
R_{f0} overall flux Richardson number (change of potential energy of the stratified fluid/total energy available for mixing)
R_{fm} global flux Richardson number (change in potential energy of the system/net available energy for mixing)
Re_l Reynolds number ($= \sigma_u l/\nu = K_l/\nu$)
Ri Richardson number ($\Delta b\, D_*^3/K^2$)
Ri_l Richardson number ($\Delta b\, D_*^3/K_l^2$)
Ri_0 Richardson number ($D_*\, \Delta b/u_*^2$)
$\widehat{Ri}$ Richardson number ($V_0^2\, D_*^2/K^2$)
$\widehat{Ri}_l$ Richardson number ($V_0^2\, D_*^2\, K_l^2$)
Ri_{**} Richardson number ($g\,(\Delta T/T)\,\delta/u_*^2$)
S stroke of the grid oscillations
t time
T temperature
u horizontal turbulent velocity within the patches (subscripts denote the regions R_1, R_2 and R_3)
u_e entrainment velocity in a stratified fluid
u_K Kolmogorov's velocity scale
u_* velocity scale characterizing the r.m.s. velocity near the interface
u_{eK} entrainment velocity by the Kolmogorov eddies
u_{el} entrainment velocity by the large-scale eddies
u, v horizontal turbulent-velocity components
V_0 $(D_0\, \Delta b_0)^{\frac{1}{2}}$ where D_0 is the initial thickness of the fresh-water layer and Δb_0 is the initial buoyancy jump
w vertical turbulent velocity within the patches (subscripts denote the regions R_1, R_2 and R_3)
w_{2f} vertical r.m.s. velocity of the flattened eddies at the density interface
w_{2i} r.m.s. velocity of the quasi-isotropic eddies
x D_*-z
y a normalizing lengthscale, $S^{\frac{3}{4}}M^{\frac{1}{4}}(\omega/N)^{\frac{1}{2}}$
z distance measured from a virtual origin
α $D_*/t^{\frac{1}{2}}$
α_i constants ($i = 1, 2$)
α_{1j} constants ($j = 1, 2$)
β constant ($l = \beta z$)
γ_1 constant
δ thickness of the turbulent boundary layer
δ_i interfacial-layer wave height (subscripts 2 and 3 denote regions R_2 and R_3)
Δb buoyancy jump across the interfacial layer
ΔT temperature jump across the interfacial layer
ϵ dissipation (subscripts 2, 3 and 21 correspond to regions R_2, R_3 and R_1 close to R_2)
ϵ_p dissipation in a patch
ζ $z-D_*$
θ temperature fluctuation
ϕ, ϕ_1 functionals
λ Taylor's microscale
ν kinematic viscosity

ρ	density
σ_u	r.m.s. horizontal velocity
ω	grid frequency
ω_i	frequency of the interfacial-layer waves
Subscripts:	'0' represents some reference condition
	$\overline{\ }$ overbar represents average

3. Some properties of oscillating-grid turbulence in a homogeneous fluid

As mentioned in §1, the integral properties of oscillating-grid turbulence in a homogeneous fluid have been extensively studied. Both theoretical and experimental investigations indicate that

$$\sigma_u \sim \frac{K}{z}, \tag{1}$$

$$l \sim z, \tag{2}$$

where z is distance from the virtual origin (near the grid), σ_u is the r.m.s. velocity (all three components are of the same order) and l is the integral scale. The 'action' parameter K in (1), which characterizes the grid and its motion, may be evaluated in two ways. If we use the definition $K_l = \sigma_u l$, then, according to Hopfinger & Toly (1976),

$$\sigma_u = C_2 M^{\frac{1}{2}} S^{\frac{3}{2}} \omega z^{-1}, \tag{3}$$

$$l = \beta z, \tag{4}$$

and $K_l = \beta C_2 M^{\frac{1}{2}} S^{\frac{3}{2}} \omega$, where C_2 is a constant, M, S, and ω are the mesh size, stroke and frequency respectively, and $\beta = \beta(S/M)$. Alternatively, the 'action' K can be evaluated by observing the increase with time of the depth D_* of a grid-induced turbulent region in a homogeneous fluid in accordance with $D_* = (Kt)^{\frac{1}{2}}$ as reported in Dickinson & Long (1983). A simple calculation yields $K \approx 7K_l$ (Fernando 1983).

Another observed property of oscillating-grid turbulence is the development of isotropy within a short distance from the grid (Hopfinger & Toly 1976). For isotropic turbulence we may write (Hinze 1975, p. 225)

$$\epsilon = 15\nu \frac{\sigma_u^2}{\lambda^2},$$

where ϵ is the dissipation function, λ is Taylor's microscale and ν is the viscosity. Also, using a familiar expression for energy dissipation,

$$\epsilon = A \frac{\sigma_u^3}{l}, \tag{5}$$

where A is a constant, we get

$$\lambda = \left(\frac{15}{A}\right)^{\frac{1}{2}} l\, Re_l^{-\frac{1}{2}}, \quad Re_l = \frac{\sigma_u l}{\nu}, \tag{6}$$

where Re_l is the Reynolds number and $A \approx 0.63$ (Bouvard & Dumas 1967). This is comparable to other estimates (Batchelor 1953), but somewhat lower than the commonly quoted value of 0.8 (Townsend 1976). Also note that, near the propagating turbulent front, turbulence cannot be isotropic (Phillips 1955), so that the above results are strictly valid only in regions some distance away.

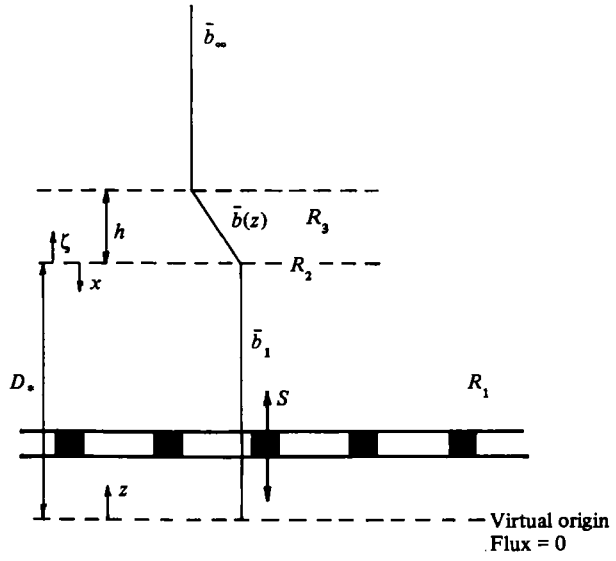

FIGURE 1. A schematic diagram of a grid oscillating in a two-layer stratified fluid with the quiescent fluid above.

The energy equation of the form (Thompson & Turner 1975),

$$-r\frac{\partial\sigma_u^3}{\partial z}-\frac{A}{\beta}\frac{\sigma_u^3}{z}=0, \tag{7}$$

where r is a universal constant, may be integrated to yield a behaviour in agreement with (1),

$$\frac{\sigma_u}{\sigma_{u_0}}=\left(\frac{z}{z_0}\right)^{-A/3\beta r}, \tag{8}$$

where 0 represents some reference distance from the grid. Using (1) and (8) together with $A\approx 0.61$ and (for Turner-type grids) $\beta=0.25$, (Hopfinger & Toly 1976), we estimate $r\approx 0.81$.

4. A review of Long's theory

For convenient comparison of experimental results and theoretical arguments, we give now a brief discussion of the theory of Long (1978*b*). The reader who is familiar with that theory may skip the details of this section and use it only for reference. The reader should notice particularly that all the arguments presented in the theory are for the case of large Richardson numbers, and so for high stabilities.

Figure 1 is a schematic view of the development of the mixed layer in a two-fluid system in which turbulence is generated by an oscillating grid. If we assume that the buoyancy† $\bar{b}_1$ in the mixed layer (region R_1) is uniform and that buoyancy varies linearly with depth in the interfacial layer of thickness h (region R_3), we may write

$$\bar{b}_1=\bar{b}_\infty+\Delta b, \tag{9}$$

† Buoyancy is defined as $b=(\rho-\rho_0)g/\rho_0$, where ρ is the density of the fluid, ρ_0 is the reference density, and g is the acceleration due to gravity.

where $\bar{b}_\infty$ is the buoyancy in the undisturbed region and Δb is the buoyancy jump across the interfacial layer. The buoyancy in R_3 is taken to be

$$\bar{b}_3(z) = \bar{b}_\infty + \Delta b - \frac{\Delta b}{h}(z - D_*), \tag{10}$$

where D_* is the thickness of the mixed layer measured from the virtual origin. If $q = -\overline{bw}$ is the buoyancy flux, we may integrate the buoyancy equation,

$$\frac{\mathrm{d}\bar{b}}{\mathrm{d}z} = \frac{\mathrm{d}q}{\mathrm{d}z}, \tag{11}$$

over the mixed layer and over a part of the interfacial layer to yield

$$q_2 = D_* \frac{\mathrm{d}\Delta b}{\mathrm{d}t}, \tag{12}$$

$$q_3 = q_2 + \frac{\mathrm{d}\Delta b}{\mathrm{d}t}\left[\zeta - \frac{\zeta^2}{2h}\right] + \Delta b\left[\frac{\zeta^2}{2h^2}\frac{\mathrm{d}h}{\mathrm{d}t} + \frac{\zeta}{h}\frac{\mathrm{d}D_*}{\mathrm{d}t}\right], \tag{13}$$

where $\zeta = z - D_*$, and R_2 is a comparatively thin region between R_1 and R_3 of thickness of order of the amplitude δ_2 of the interfacial waves.† Since $q_3 = 0$ at $\zeta = h$, (12) and (13) give a fundamental constant for the problem:

$$V_0^2 = (D_* + \tfrac{1}{2}h)\,\Delta b. \tag{14}$$

Based on the experimental observations, it is assumed that the interfacial layer consists of intermittent turbulent patches caused by sporadic breaking of internal waves, and the patches at the entrainment interface which connect the interfacial region to the mixed region are responsible for the turbulent transfer of buoyancy to the mixed layer. The turbulent-velocity components u, v, w within the patches should be of the same order while the turbulence is active, and we may write for the region R_3,

$$q_3 = -B_1 u_3 b_3 I_3, \tag{15}$$

where u_3, b_3 are r.m.s. velocity and buoyancy fluctuations in the patches, I_3 is the intermittency and we denote universal constants by B_1, B_2, ... Also we assume that a turbulent patch generated by wave-breaking in a linearly stratified interfacial layer has the property that within it the potential energy $\delta_3 b_3$ (where δ_3 is the vertical dimension of the patch) is of the order of the kinetic energy u_3^2, i.e.

$$u_3^2 = B_2 \delta_3 b_3 = B_3 \delta_3^2 \left(\frac{\Delta b}{h}\right). \tag{16}$$

This assumption in Long's theory has apparently been verified recently by Liu (1982), who found $B_3 \approx 0.46$. If we now assume for the dissipation ϵ_p in the patches the form

$$\epsilon_\mathrm{p} = B_4 \frac{u_3^3}{\delta_3}, \tag{17}$$

we have

$$\epsilon_3 = B_4 \frac{u_3^3}{\delta_3} I_3. \tag{18}$$

† R_2 and δ_2 are assumed to become smaller and smaller as the Richardson number $Ri = D_*^3\,\Delta b/K^2$ becomes large. Some r.m.s. quantities like vertical velocity w and mean buoyancy b are assumed to vary little across R_2; others like r.m.s. horizontal velocities u, v and gradient $\mathrm{d}\bar{b}/\mathrm{d}z$ are assumed to vary rapidly across the layer. Buoyancy flux q must be continuous to avoid infinite values of $\partial\bar{b}/\partial t$ from (11).

Notice that if we define as the Ozmidov (1965) length

$$l_0 \sim \epsilon_p^{\frac{1}{2}} \Big/ \left(\frac{\Delta b}{h}\right)^{\frac{3}{4}}, \tag{19}$$

we find that $\delta_3 \sim l_0$. Notice the important points of this discussion, that, to make physical sense, the Ozmidov length in intermittent turbulence should be defined in terms of ϵ_p rather than ϵ, i.e. $l_0 \sim \epsilon_p^{\frac{1}{2}}/N^{\frac{3}{2}}$, where N is the buoyancy frequency, and that it is proportional to the vertical size of the turbulent patches. Using (15), (16) and (18), we obtain

$$\frac{\delta_3}{h} = B_3^{-\frac{1}{2}} \frac{u_3}{(h\,\Delta b)^{\frac{1}{2}}} \quad \text{or} \quad \frac{u_3}{\delta_3} = B_3^{\frac{1}{2}} \left(\frac{\Delta b}{h}\right)^{\frac{1}{2}}, \tag{20}$$

$$q_3 = -\frac{B_1 B_3^{\frac{1}{2}}}{B_2} u_3^2 \left(\frac{\Delta b}{h}\right)^{\frac{1}{2}} I_3, \tag{21}$$

$$\epsilon_3 = B_4 B_3^{\frac{1}{2}} u_3^2 \left(\frac{\Delta b}{h}\right)^{\frac{1}{2}} I_3. \tag{22}$$

We note the following.

(*a*) Equation (20) shows that the frequency of the eddies (u_3/δ_3) in the interfacial layer is of the same order as the local buoyancy frequency, $N_1 = (\Delta b/h)^{\frac{1}{2}}$, and this makes possible the resonant breaking of waves when the amplitude becomes of the order of the wavelength (Long 1970; Phillips 1977; Fernando 1983).

(*b*) Equations (21) and (22) show that

$$q_3 = -B_1 B_4^{-1} B_2^{-1} \epsilon_3 \quad \text{or} \quad q_3 \sim \epsilon_3.$$

Since the energy balance in the interfacial layer may be written

$$-\frac{\partial \mathscr{F}_3}{\partial z} - (\overline{bw})_3 - \epsilon_3 = 0, \tag{23}$$

where $\mathscr{F}$ is the diffusive energy flux, and since $(\overline{bw})_3$ and ϵ_3 are of the same order and are both energy sinks, we infer that

$$-\frac{\partial \mathscr{F}_3}{\partial z} \sim (\overline{bw})_3 \sim \epsilon_3. \tag{24}$$

For future purposes we may also write†

$$A_2 \frac{\partial u_3^3}{\partial z} = q_3, \tag{25}$$

$$\frac{\partial u_3^3}{\partial z} = B_7 q_3, \quad A_2 = \frac{1}{B_7}. \tag{26}$$

(*c*) The average buoyancy flux in the interfacial layer ($\bar{q}_3$) can be evaluated in two ways. Averaging (25) yields

$$\bar{q}_3 h = -A_2 w_2^3, \tag{27}$$

† Long (1978*b*) introduced the notation $A_1, A_2, \ldots$ to permit such 'constants' to vary with the stability of the undisturbed layer in case that layer was not homogeneous. Here the As and Bs are all universal constants.

where w_2 is the vertical velocity of the eddies in the turbulent patches of the region R_2. Then, averaging (13) and substituting from (12) and (27), we get

$$-\frac{A_2 w_2^3}{h} = D_* \frac{\mathrm{d}\Delta b}{\mathrm{d}t} + \frac{h}{3}\frac{\mathrm{d}\Delta b}{\mathrm{d}t} + \frac{\Delta b}{6}\frac{\mathrm{d}h}{\mathrm{d}t} + \frac{\Delta b}{2}\frac{\mathrm{d}D_*}{\mathrm{d}t}. \tag{28}$$

The corresponding equations for (20) and (21) for the region of the entrainment interface (region R_2) become

$$\frac{\delta_2}{h} = B_3^{-\frac{1}{2}} \frac{w_2}{(h\,\Delta b)^{\frac{1}{2}}}, \tag{29}$$

$$\frac{B_1}{B_2} B_3^{\frac{1}{2}} I_{23} w_2^2 \left(\frac{\Delta b}{h}\right)^{\frac{1}{2}} = -D_* \frac{\mathrm{d}\Delta b}{\mathrm{d}t}. \tag{30}$$

In (29) and (30), w_2 and δ_2 are well defined in R_2, and I_{23} is the intermittency in the region of R_3, close to the entrainment interface R_2 (figure 1).

To evaluate w_2 it is necessary to consider two types of eddies in the mixed layer near the interface: the energy-containing eddies, which are flattened at the density interface with vertical velocities of order $w_{2f} \sim Kx/D_*^2$, where $x = D_* - z$; and the quasi-isotropic eddies of size δ_2 (which do not feel the presence of the interface), with vertical velocities w_{2i} determined by Kolmogorov's law as $w_{2i} \sim \epsilon_{21}^{\frac{1}{3}} \delta_2^{\frac{1}{3}}$, where ϵ_{21} is the dissipation in the region of R_1 that is close to the entrainment interface R_2. Since the flattening of the large eddies does not affect the large-wavenumber region of the energy spectrum, we may write $\epsilon_{21} \sim K^3/D_*^4$, and hence $w_{2i} \sim K\delta_2^{\frac{1}{3}}/D_*^{\frac{4}{3}}$. Since $w_{2i} \gg w_{2f}$ we infer that $w_2 \sim w_{2i}$.

We may now write

$$\frac{w_2^3}{\delta_2}\frac{D_*^4}{K_l^3} = B_6. \tag{31}$$

The dissipation ϵ_p in the turbulent patches in the interfacial layer is of order u_3^3/δ_3. Since this quantity is independent of the Richardson number $Ri = D_*^3 \Delta b/K^2$ at the entrainment interface, Long argued that it should remain independent of Ri throughout R_3, but of course ϵ_p should depend on ζ/D_*.†

We get

$$\frac{u_3^3}{\delta_3} = \frac{K_l^3}{D_*^4}\phi\left(\frac{\zeta}{D_*}\right), \tag{32}$$

or, using (20),

$$u_3^3 = \left(\frac{h}{\Delta b}\right)^{\frac{3}{4}} \frac{K_l^{\frac{9}{4}}}{D_*^6} \phi_1\left(\frac{\zeta}{D_*}\right). \tag{33}$$

Alternatively, u_3^3 can be evaluated by integrating (26) across the interfacial layer and using (13). We get

$$u_3^3 = w_2^3 + B_7\left[q_2\zeta + \frac{\mathrm{d}\Delta b}{\mathrm{d}t}\left(\frac{\zeta^2}{2} - \frac{\zeta^3}{6h}\right) + \Delta b\left(\frac{\zeta^3}{6h^2}\frac{\mathrm{d}h}{\mathrm{d}t} + \frac{\zeta^2}{2h}\frac{\mathrm{d}D_*}{\mathrm{d}t}\right)\right]. \tag{34}$$

Comparison of (33) and (34) shows that

$$\phi_1\left(\frac{\zeta}{D_*}\right) = B_6^{\frac{3}{4}} B_3^{-\frac{3}{4}} - A_3\left(\frac{\zeta}{D_*}\right) + A_4\left(\frac{\zeta^2}{D_*^2}\right) + A_5\left(\frac{\zeta^3}{D_*^3}\right). \tag{35}$$

† This argument implies that ϵ itself is discontinuous across R_2.

Equating coefficients and using (12), we get

$$D_* \frac{\mathrm{d}\Delta b}{\mathrm{d}t} = -\frac{A_3}{B_7}\left(\frac{h}{\Delta b}\right)^{\frac{3}{4}} \frac{K_l^{\frac{9}{2}}}{D_*^7}, \tag{36}$$

$$\frac{D_*}{2}\frac{\mathrm{d}\Delta b}{\mathrm{d}t} + \frac{\Delta b}{2h} D_* \frac{\mathrm{d}D_*}{\mathrm{d}t} = \frac{A_4}{B_7}\left(\frac{h}{\Delta b}\right)^{\frac{3}{4}} \frac{K_l^{\frac{9}{2}}}{D_*^7}, \tag{37}$$

$$\frac{-D_*^2}{6h}\frac{\mathrm{d}\Delta b}{\mathrm{d}t} + \frac{D_*^2}{6h^2}\Delta b \frac{\mathrm{d}h}{\mathrm{d}t} = \frac{A_5}{B_7}\left(\frac{h}{\Delta b}\right)^{\frac{3}{4}} \frac{K_l^{\frac{9}{2}}}{D_*^7}. \tag{38}$$

Also (28) together with (29) and (31) give

$$\frac{-A_2 B_6^{\frac{3}{2}} B_3^{-\frac{3}{4}} K_l^{\frac{9}{2}}}{h^{\frac{1}{4}} D_*^6 (\Delta b)^{\frac{3}{4}}} = D_* \frac{\mathrm{d}\Delta b}{\mathrm{d}t} + \frac{h}{3}\frac{\mathrm{d}\Delta b}{\mathrm{d}t} + \frac{\Delta b}{6}\frac{\mathrm{d}h}{\mathrm{d}t} + \frac{\Delta b}{2}\frac{\mathrm{d}D_*}{\mathrm{d}t}. \tag{39}$$

Equations (36)–(39) and (14) together with the initial conditions determine the problem. Although there are 5 equations in 3 unknowns, D_*, h and Δb, if we impose the condition that $D_* = 0$ at $t = 0$, we find the unique solution if we accept certain relationships between the various constants. The results expressed in terms of K_l are

$$D_* = B_8 V_0^{-\frac{7}{11}} K_l^{\frac{9}{11}} t^{\frac{8}{11}}, \tag{40}$$

$$h = \alpha_1 D_*, \quad \Delta b = \frac{2V_0^2}{(2+\alpha_1) D_*}, \tag{41}$$

$$\frac{u_e D_*}{K_l} = \alpha_2 Ri_l^{-\frac{1}{4}}, \quad \alpha_2 = \frac{6A_2 B_6^{\frac{3}{2}}}{\alpha_1^{\frac{1}{4}} b_3^{\frac{3}{4}}(3+\alpha_1)}, \tag{42}$$

where $Ri_l = \Delta b\, D_*^3/K_l^2$ and $u_e = \mathrm{d}D_*/\mathrm{d}t$ is the entrainment velocity. Also

$$\frac{w_2 D_*}{K_l} = \alpha_4 Ri_l^{-\frac{1}{4}}, \quad \alpha_4 = \frac{B_6^{\frac{1}{2}} \alpha_1^{\frac{1}{4}}}{B_3^{\frac{1}{4}}}, \tag{43}$$

$$\frac{\delta_2}{D_*} = \alpha_5 Ri_l^{-\frac{3}{4}}, \quad \alpha_5 = \frac{B_6^{\frac{1}{2}} \alpha_1^{\frac{3}{4}}}{B_3^{\frac{3}{4}}}, \tag{44}$$

$$I_{23} = \alpha_6 Ri_l^{-\frac{3}{4}}, \quad \alpha_6 = \frac{6A_2 B_6^{\frac{1}{2}} B_2}{B_1 \alpha_1^{\frac{1}{4}} B_3^{\frac{3}{4}}(3+\alpha_1)}. \tag{45}$$

Finally, the r.m.s. buoyancy fluctuations in the mixed layer (b_1) and in the region of R_2 close to the mixed layer (b_{23}) are given by†

$$\frac{b_1}{\Delta b} \sim Ri_l^{-\frac{1}{4}} \quad \text{and} \quad \frac{b_{23}}{\Delta b} \sim Ri_l^{-\frac{3}{4}}. \tag{46), (47}$$

5. Experimental procedure

The basic experimental set-up and the bulk of the experimental procedure is discussed fully in Fernando & Long (1983) and shown schematically in figure 2. The buoyancy measurements in the mixed layer and interfacial layer were made by using stationary single-electrode conductivity probes; the density/depth profiles were made using a travelling probe. The visual observations of the interfacial-layer structure were made on a shadowgraph either by normal or laser light. At various

† Long's paper has $b_{23}/\Delta b \sim Ri^{-\frac{1}{4}}$. This is an error; the exponent should be $-\frac{3}{4}$ as in (47).

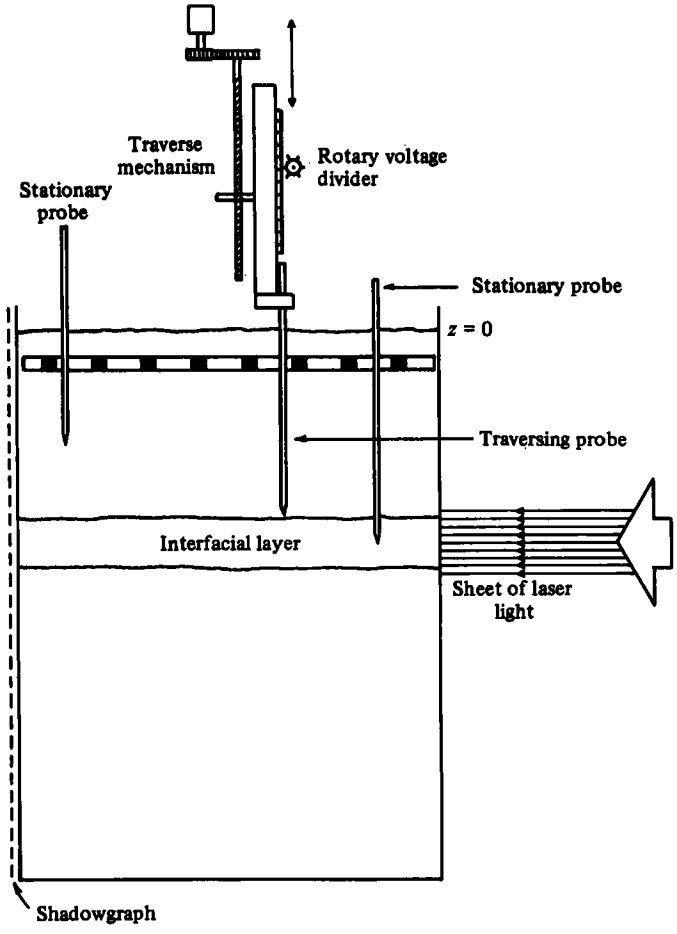

FIGURE 2. A schematic view of the experimental apparatus.

depths of the mixed layer and under specially adjusted lighting conditions, the interfacial layer was filmed by a 16 mm camera. Wave data (both frequency and amplitude) were obtained either from frame-by-frame analysis of the ciné film in a manner described by Wyatt (1978) or by direct observations of the shadowgraph. Usually, the wave height or frequencies at a given depth were calculated by analysing fifteen waves or so and taking the average.

6. The interfacial layer

6.1. *Qualitative observations*

Visual observations were made over extended periods on a shadowgraph using either a normal beam of light emerging from a parabolic reflector or a vertical sheet of laser light. The interfacial layer was clearly visible and was seen to be separated from the well-mixed layer and the quiescent layer by oscillating thin boundary regions possessing strong curvature of its density profile. The region of strong density profile curvature at the entrainment zone appears distinctly as a thin, wavy, white streak in figures 3 and 4 and less distinctly in figures 5 and 6. The fluid near the mixed-layer–interfacial-layer boundary is carried to the upper, well mixed layer by

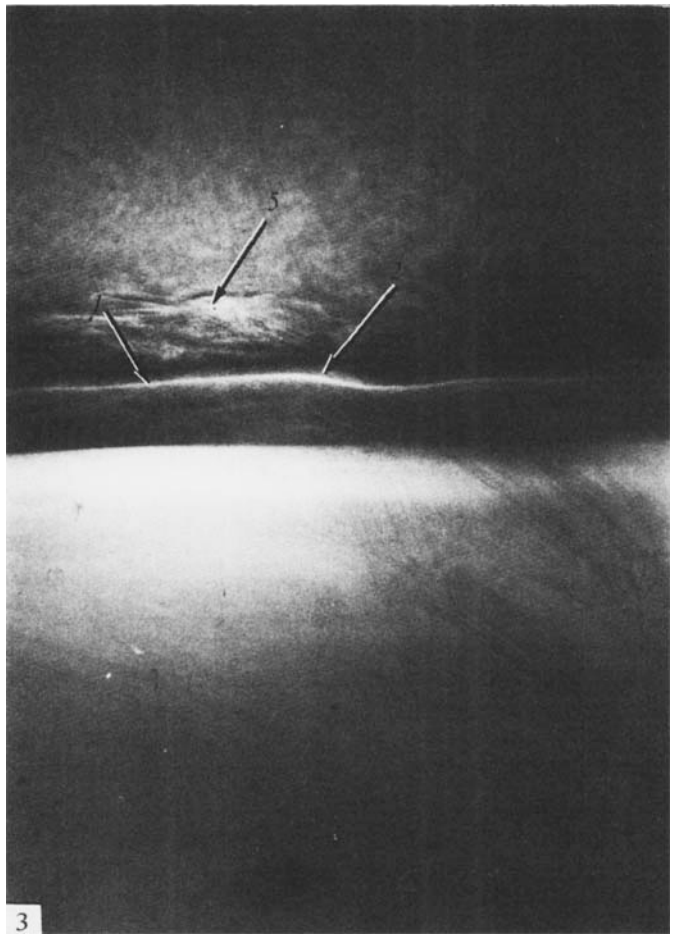

FIGURE 3. Shadowgraph observations of the entrainment interface. (The grid is located in the upper mixed layer.) In figures 3–8 the numbers on the photographs have the following meanings: 1, region of maximum curvature in density; 2, entrainment interface; 3, bottom of the interfacial layer; 4, internal-wave structure in the interfacial layer; 5, rising dense fluid; 6, structure of the impinging eddies on the entrainment interface; 7, oscillations of the bottom of the interfacial layer; 8, homogeneous mixed layer; 9, steepening of an interfacial wave.

scouring or splashing by the large-scale eddies impinging on it. The large eddies encounter the region of maximum density gradient and then flatten and bounce back. During this process, the fluid is ejected into the mixed layer. Figures 5 and 6 depict the ripple-like structure caused by impinging mixed-layer eddies appearing in the region just above the region of strong density-profile curvature.

From the foregoing discussion, it seems that the entrainment at a density interface is caused by the breaking of interfacial waves, rising of the mixed fluid formed by the patches on the entrainment interface to the top of the interfacial layer and then ejection of this fluid into the mixed layer by the scouring and splashing action of the large-scale, energy-containing eddies. Figures 7 and 8 show the observations of the interfacial layer on a shadowgraph by a vertical sheet of laser light. Note the wave structure inside it and the oscillation of the bottom of the interfacial layer.

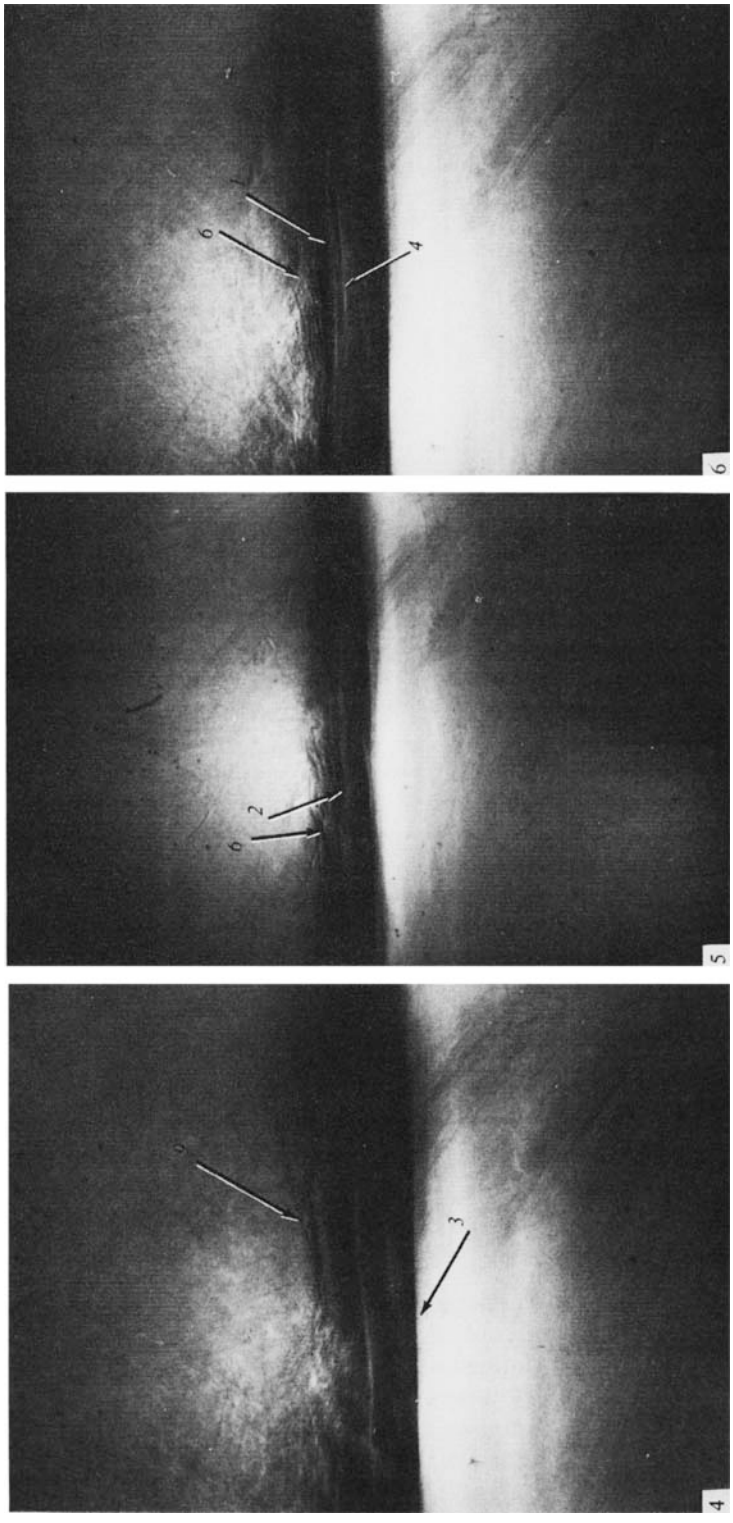

FIGURES 4, 5 AND 6. Shadowgraph observations of the entrainment interface. (The grid is located in the upper mixed layer.)

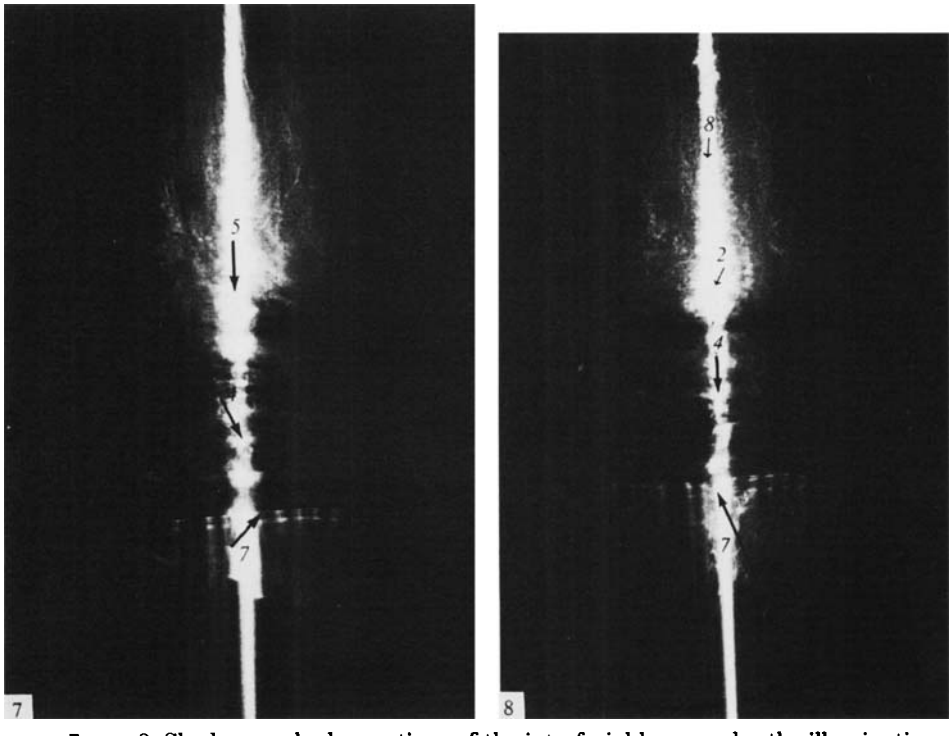

FIGURES 7 AND 8. Shadowgraph observations of the interfacial layer under the illumination of a vertical sheet of laser light. (The grid is located in the upper mixed layer.)

6.2. *Energy budget*

According to (24), the buoyancy flux, the dissipation and the energy-flux divergence in the interfacial layer are all of the same order. In the present experiment, the buoyancy flux at the interface was evaluated by differentiating the curve of Δb versus t obtained by a cubic-spline fit to the Δb versus t data and then using (12). Dissipation ϵ_{21} in the region of R_1 close to the entrainment interface (figure 1) was calculated using (5) and $\sigma_u = K_l/\beta D_*$, $l = \beta D_*$. Figure 9 shows a plot of $\overline{bw}$ versus ϵ, as calculated, indicating proportionality with $\overline{bw}/\epsilon \approx 1.75$. Since they are both sinks and are proportional, the energy-flux divergence in the upper part of R_1 must also be proportional to $\overline{bw}$ according to (23). Figure 10 shows the variation of the energy-flux divergence with the buoyancy flux. We find the ratio

$$\overline{bw}\Big/\left(-\frac{\partial \mathscr{F}}{\partial z}\right) \approx 0.65. \tag{48}$$

Notice that (48) is the diffusive-flux Richardson number R_{fd}, which is the zero-mean-shear counterpart of the commonly used flux Richardson number R_f for stratified turbulent shear flows. R_f is defined as the ratio of buoyancy flux to the local shear production of turbulent kinetic energy. In the context of oscillating-grid turbulence, R_{fd} was first used by Hopfinger & Linden (1982).

It is worthwhile to mention the evaluations of Linden (1979, 1980) of still another flux Richardson number. By dropping a grid through a density interface, he produced turbulent mixing, and a flux Richardson number R_{f0} was evaluated as the ratio of the change in potential energy of the system to the energy available for mixing. His

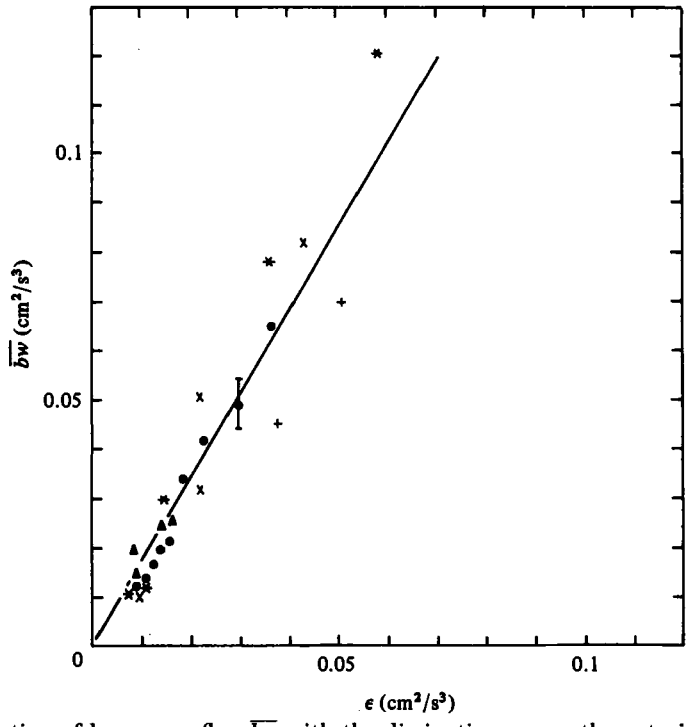

FIGURE 9. Variation of buoyancy flux $\overline{bw}$ with the dissipation ϵ near the entrainment interface: ▲, $V_0 = 19.53$, $K = 18.81$; ×, 20.22, 18.70; *, 22.83, 17.74; +, 25.67, 15.52, ●, 25.80, 1.95 (V_0 in cm/s, K in cm²/s).

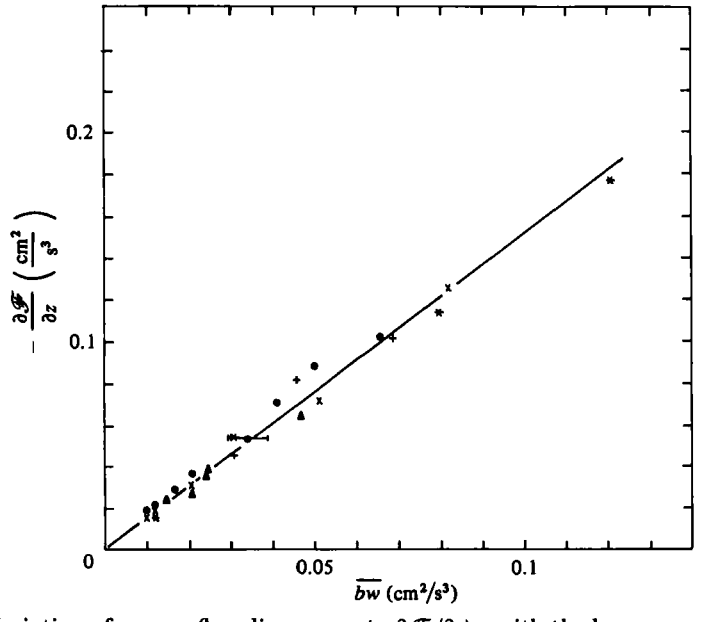

FIGURE 10. Variation of energy-flux divergence $(-\partial \mathcal{F}/\partial z)_{21}$ with the buoyancy flux $\overline{bw}$ at the entrainment interface. The symbols have the same meaning as in figure 9.

observations indicate that, as the overall Richardson number Ri_0 (defined below) increases, R_{f0} first increases, comes to a maximum and then decreases. McEwan (1983) argued that this behaviour may be explained by considering the variation of loss to viscous dissipation in the large-scale motions (which does not contribute to the mixing) with varying stability. He also showed that, if the flux Richardson number R_{fm} is defined as the ratio of the change in potential energy to the net energy available for mixing (i.e. total energy supplied less the viscous dissipation at large scales), then R_{fm} tends to be a constant. The observed values of R_{fm} are much less than R_{f0}, and this discrepancy needs an explanation. Note that both R_{f0} and R_{fm} have the nature of a global flux Richardson number, whereas R_{fd} in the present work is local.

Linden's (1979) results may also be interpreted in a different qualitative way. For our present experiments, as in Linden's experiments, in which the interfacial-layer thickness is a constant fraction of the mixed-layer depth, we may still write

$$R_{f0} \propto \frac{u_e}{u_*} Ri_0, \tag{49}$$

as in Linden (1979), where R_{f0} is Linden's flux Richardson number, defined above, u_* is a characteristic velocity scale for entrainment, representing the r.m.s. turbulence velocity near the interface, and $R_0 = D_* \Delta b / u_*^2$. A plot of $R_{f0}/Ri_0 \propto u_e/u_*$ versus Ri_0 for several different experiments is shown in figure 11. We note the following.

(*a*) At low values of Ri_0 the entrainment coefficient is independent of Ri_0, indicating that the large-scale, energy-containing eddies are responsible for entrainment. In this case the large eddies do not flatten at the interface, and Long's arguments are not valid in determining entrainment rates. The criterion for eddy flattening is discussed in §8.3.

(*b*) At high values of Ri_0 the entrainment coefficient shows a power-law dependency on Ri_0. The $-\frac{7}{4}$ line is drawn to indicate Long's (1978*b*) prediction for grid-generated mixed-layer growth in two-fluid systems.

6.3. *Interfacial-layer thickness*

The development of the interfacial layer of thickness h was observed (i) using a sheet of laser light (e.g. figures 7 and 8). In this case the interfacial-layer thickness h_1 is defined as the estimated average distance between the two points where maximum curvature of the density profile can be observed; (ii) plotting salinity/depth measurements from a travelling conductivity probe, fitting a least-squares fit to the central 70% of the data points in the interface and extending this line until it intersects the mean salinities in the upper and lower layers (for more details see Crapper & Linden 1974). For this case the definition of the interfacial-layer thickness h_2 is the distance between these intersection points measured along the axis corresponding to the probe traverse; (iii) using the buoyancy-conservation equation (14), together with the assumption that the interfacial-layer thickness h_3 varies with D_* as $h_3 = \alpha_{13} D_*$, where α_{13} is a constant.

(i) *Using a sheet of laser light.* The variation of h_1/D_* with the Richardson number when measured with the laser-beam technique is shown in figure 12. At high Ri the ratio $\alpha_{11} = h_1/D_*$ tends to a constant value of approximately 0.15.

(ii) *Using a travelling conductivity probe.* Figure 13 shows the variation of $\alpha_{12} = h_2/D_*$ with Ri when measured using the conductivity probe. Although at small Ri results show considerable scatter, h_2/D_* seems to tend to a constant value at high Ri. A possible explanation for such scatter could be the presence of large excursions of the interfacial layer at low Ri, so that an instantaneous density profile is not a

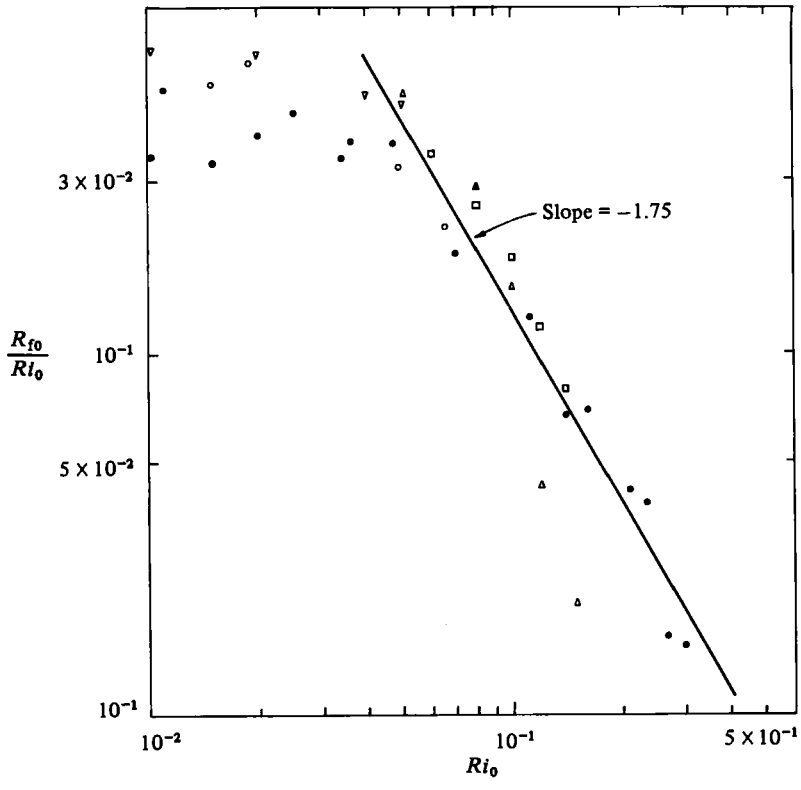

FIGURE 11. Variation of R_{f0}/Ri_0 with the overall Richardson number Ri_0. The symbols have the same meaning as in Linden (1979).

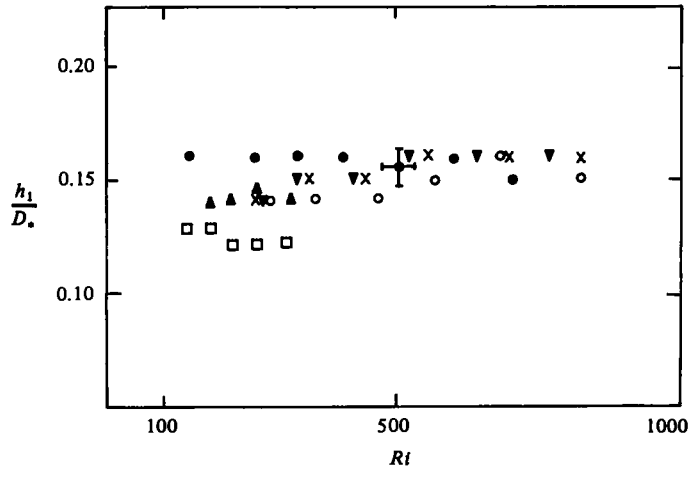

FIGURE 12. Variation of h_1/D_* with the Richardson number Ri measured by the laser-beam technique: □, $V_0 = 13.38$, $K = 18.40$; ▲, 15.22, 18.52; ●, 20.58, 18.52; ▼, 21.8, 18.4; ○, 23.09, 18.40; ×, 24.38, 18.40 (V_0 in cm/s, K in cm²/s).

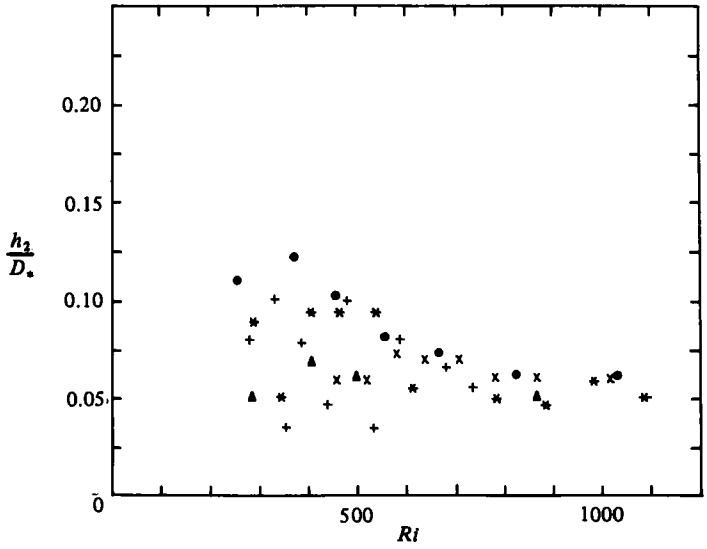

FIGURE 13. Variation of h_2/D_* with the Richardson number Ri measured by a travelling conductivity probe: +, $V_0 = 1.53$, $K = 18.81$; ●, 20.22, 18.74; ▲, 22.8, 1.74; ×, 25.80, 18.95; *, 25.50, 15.52 (V_0 in cm/s, K in cm²/s).

good indicator of the average profile. To verify this, at each mixed-layer depth, several density profiles were taken (usually five) and the interfacial-layer thicknesses were calculated for each of them. The resulting h_2/D_* values together with their averages are shown in figure 14. The constancy of the average value of h_2/D_* indicates that the instantaneous profiles cannot be used as an indicator of the average density profile, especially at low Ri. The measured average $\alpha_{12} = h_2/D_*$ ratio of 0.06–0.07 is considerably less than that obtained from laser observations. In part this may be due to the difference in the definition of the interfacial layer. As indicated above, the conductivity-probe technique neglects the end curvature of the density profiles. Observations by Crapper & Linden (1974) are rather different from ours and indicate that there is no significant difference between their averaged and instantaneous density profiles. This may perhaps be due to the quasi-steady and symmetric nature of their experiments, in which the measurements were made with both homogeneous layers stirred at the same frequency. Notice also that our h_2/D_* values are considerably less than the measurements of Crapper & Linden, but comparable to those of Moore & Long (1971) (0.08) and Wolanski & Brush (1975) (0.062).

(iii) *Using the buoyancy-conservation equation.* Using (14) together with Long's (1978*b*) solution (41) in the form $h_3 = \alpha_{13} D_*$, we may write

$$D_*(1+\tfrac{1}{2}\alpha_{13}) = V_0^2/\Delta b. \tag{50}$$

A log–log plot of $V_0^2/\Delta b$ versus D_* is shown in figure 15, and shows good agreement with (50). The value of $\alpha_{13} \approx 0.22$ obtained in this way is much higher than that obtained from either of methods (i) or (ii) but is comparable to the observations of Deardorff, Willis & Stockton (1980) (0.21) and Price (1979) (0.30). Deardorff *et al.* defined the interfacial-layer thickness as the distance between the two points where turbulent buoyancy flux is zero and where only a small percentage of the fluid remains unmixed. This is consistent with the definitions of Long's (1978*b*) theory. Price has not clearly defined his interfacial-layer thickness.

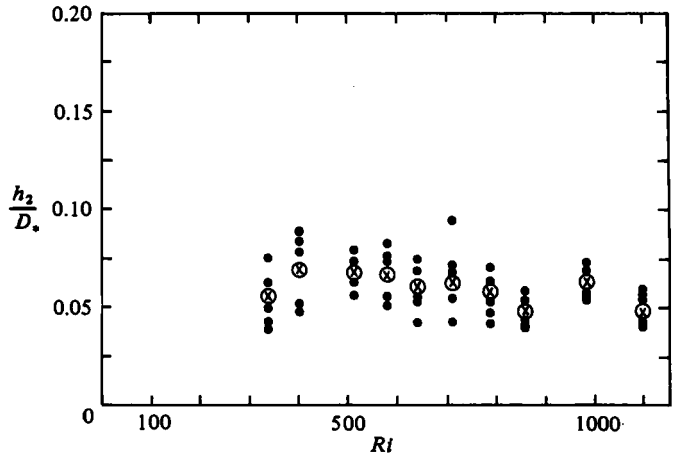

FIGURE 14. Variation of h_2/D_* with the Richardson number measured by a travelling conductivity probe: ● represents the measured values using the instantaneous conductivity/depth profiles, and ⊗ represents their averaged value at a given Ri.

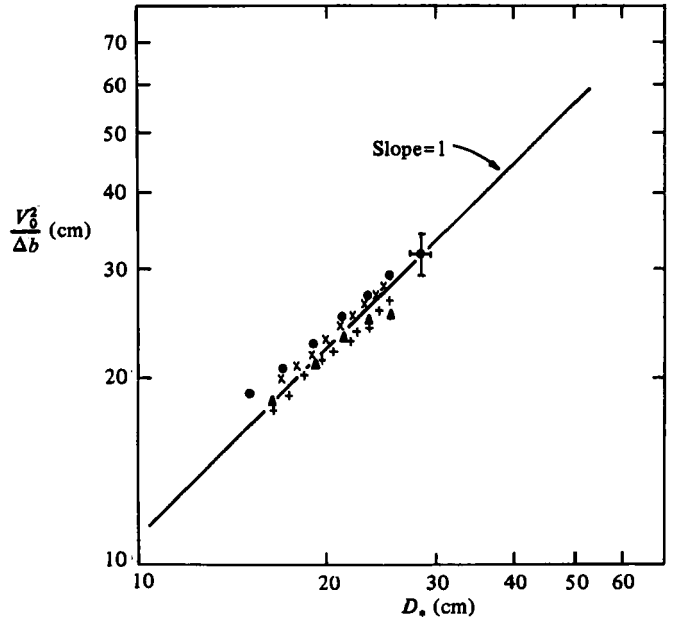

FIGURE 15. A log–log plot of $V_0^2/\Delta b$ versus D_*. Symbols have the same meaning as in figure 13.

6.4. *Buoyancy transfer at the entrainment interface*

(*a*) *Turbulent transport of buoyancy*

We may show that the eddy–diffusivity concept is useful even in the strongly stratified interfacial layer by defining eddy diffusivity K_e by the equation

$$-q_2 = K_e \frac{d\bar{b}}{dz}. \tag{51}$$

According to Long's theory, $q_2 = B_1 I_{23} w_2 b_{23}$ and $b_{23} = B_3 B_2^{-1} \delta_2 \, \mathrm{d}\bar{b}/\mathrm{d}z$, so that

$$K_e = \frac{B_3 B_1}{B_2} w_2 \delta_2 I_{23}, \tag{52}$$

revealing that, with the definition implied by (51), eddy diffusivity is the product of the characteristic velocity and length, as is conventional, but now multiplied by the intermittency. According to (43)–(45) from Long's theory,

$$-\frac{q_2}{\mathrm{d}\bar{b}/\mathrm{d}z} = K_e \sim K_l Ri^{-\frac{7}{4}}. \tag{53}$$

The ratio K_e/K_l has been found from our data, and is plotted in figure 16, showing an excellent agreement with (53). Our discussion indicates that the difficulty with eddy diffusivity experienced by Linden (1979) is overcome by assuming that the quasi-isotropic eddies are involved in entrainment and by taking intermittency into account.

(*b*) *Molecular transfer of buoyancy*

In addition to the turbulent transport discussed above, buoyancy transfer across an entrainment interface may also occur by molecular diffusion. Crapper & Linden (1974) reported that at low Péclet numbers the entrainment is entirely molecular-diffusive in nature and the interfacial layer resembles a diffusive core. Turner (1965), in a study of both heat and salt transfer across a density interface, has found that at small interfacial stabilities heat and salt are transported by the turbulent eddies, whereas at high stabilities the molecular mechanisms dominate. Assuming that the large-scale eddies are responsible for entrainment, Phillips (1977) has argued that when $Ri_0 > (u_e/u_*)\,(u_* D_*/k_s)$ molecular mechanisms should take over the entrainment process (k_s is the molecular diffusivity of the stratifying agent).

In the present experiments, the Péclet number is of order 10^5 and could not vary over a substantial range. However, the total buoyancy flux q_T and the molecular diffusive flux q_d were determined (molecular-diffusive flux was determined by measuring $\mathrm{d}\bar{b}/\mathrm{d}z$ in the interfacial layer and using $q_d = k_s \, \mathrm{d}\bar{b}/\mathrm{d}z$) as a function of Richardson number. A plot of q_T/q_d (Nusselt number) versus Ri is shown in figure 17. Note that at moderate Richardson numbers the molecular fluxes are negligibly small, but increase as Ri increases.

6.5. *Wave measurements at the entrainment interface*

(*a*) *Frequency measurements*

The frequency of the interfacial-layer waves ω_i is of the same order as the buoyancy frequency in the layer. Using (43) and (44), we may write the non-dimensional frequency as

$$\frac{w_2}{\delta_2}\frac{D_*^2}{K_l} = \omega_i \frac{D_*^2}{K_l} = \frac{\alpha_4}{\alpha_5} Ri_l^{\frac{1}{2}}. \tag{54}$$

As mentioned in §5, the periods of the interfacial-layer waves were determined, and a log–log plot of $\omega_i D_*^2/K_l$ versus $Ri_l\,(= V_0^2 D_*^2/K_l^2)$ is shown in figure 18. The ratio α_4/α_5 determined in this way is about 1.42, compared with 0.66 obtained by Fernando & Long (1983) by observing the conductivity fluctuations at the upper part of the interfacial layer. The difference in the constants of proportionality is unexplained.

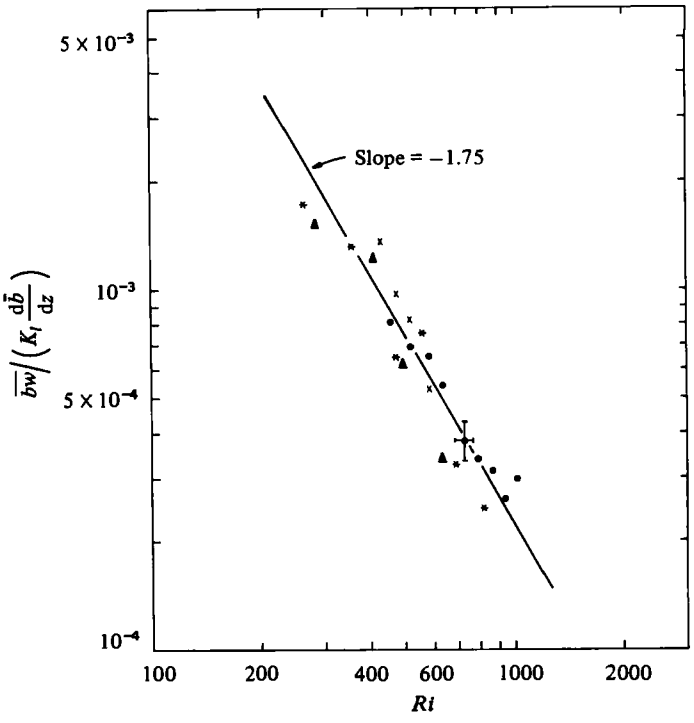

FIGURE 16. A log–log plot of $\overline{bw}/(K_l\, d\bar{b}/dz)$ versus Richardson number Ri: ×, $V_0 = 19.52, K = 18.81$; ▲, 20.22, 18.70; *, 22.83, 18.74; ●, 25.80, 18.95 (V_0 in cm/s, K in cm²/s).

(*b*) *Amplitude measurements*

The amplitude of the waves at the entrainment interface was measured as also mentioned in §5. A log–log plot of δ_2/D_* versus Ri_l is shown in figure 19. The data show considerable scatter, but indicate a decreasing trend, perhaps as $Ri_l^{-\frac{3}{4}}$ as in Long's (1978*b*) theory. The line drawn corresponds to (44), where α_5 was evaluated using an alternative technique which will be discussed in §7.

6.6. *Intermittent nature of the interfacial layer*

It has been observed both in the laboratory (Crapper & Linden 1974) and in field situations (Grant, Moilliet & Vogel 1968; Thorpe 1977; Dillon & Powell 1979) that stable layers consist of turbulent patches. Long (1978*b*) argued that these patches are caused by sporadic breaking of internal waves in the interfacial layer. His solution for the intermittency in the interfacial layer from (45) may be rewritten together with (15) as

$$I = \frac{\overline{bw}}{b_3 u_3} = B_1 \alpha_6 Ri_l^{-\frac{3}{4}}. \tag{55}$$

The recent experimental measurements of Piat & Hopfinger (1981) in a boundary layer, topped by a density interface, may be used to find the intermittency in their interfacial layer at a position where it is strongly affected by boundary-layer turbulence. Also, since the turbulent-energy supply near the edge of the boundary layer is primarily from diffusive flux (Townsend 1976), the flow situation of Piat & Hopfinger (1981) has some similarity to oscillating-grid turbulence, in which diffusive

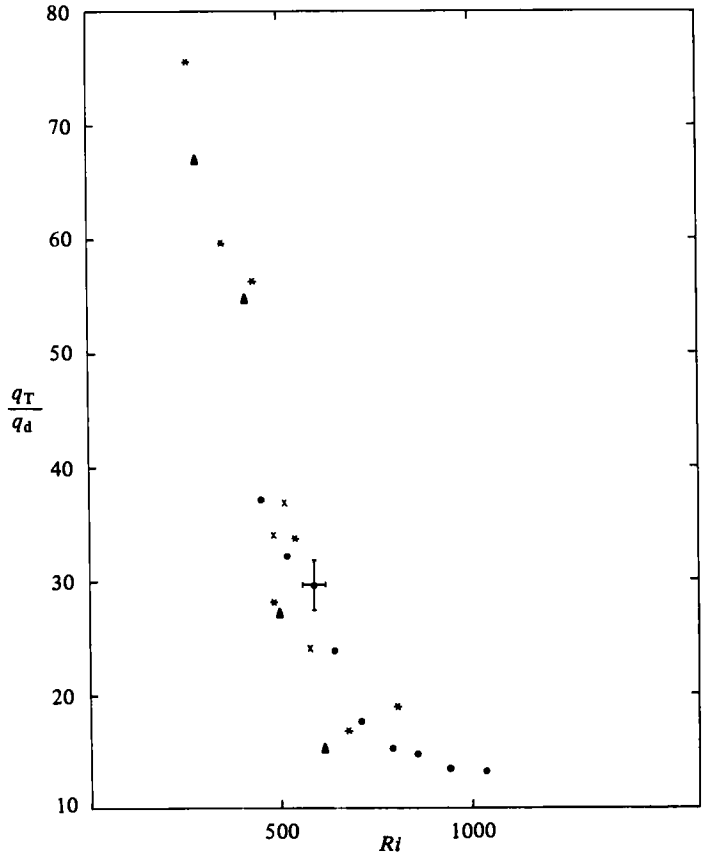

FIGURE 17. Variation of q_T/q_d with Richardson number Ri. Symbols have the same meaning as in figure 16.

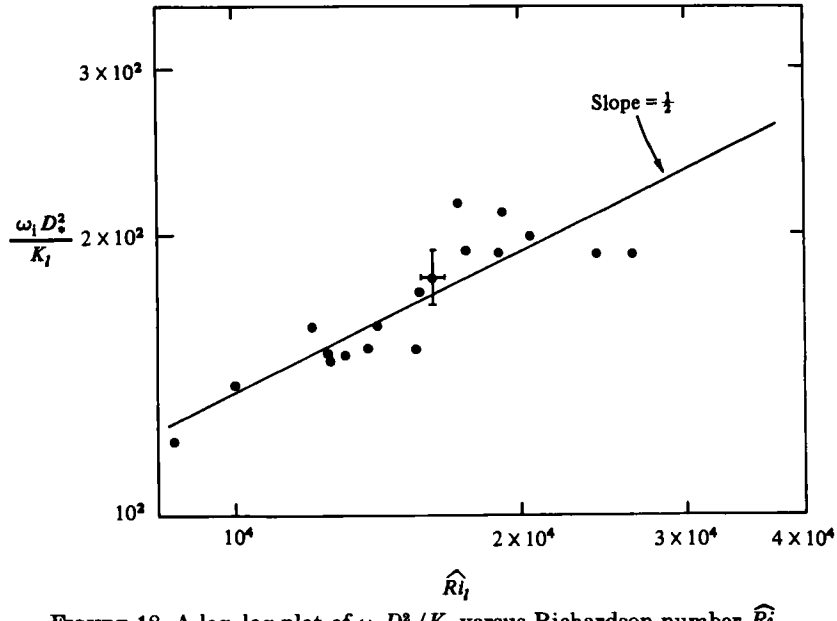

FIGURE 18. A log–log plot of $\omega_i D_*^2/K_l$ versus Richardson number $\widehat{Ri}_l$.

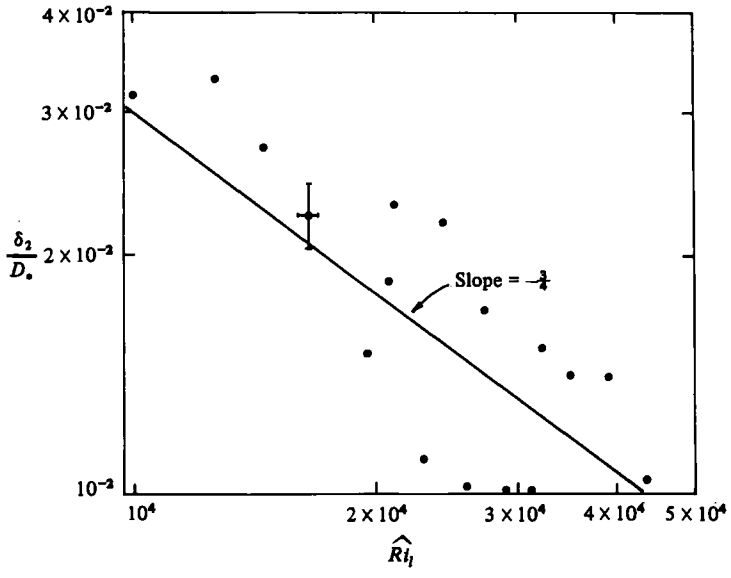

FIGURE 19. A log–log plot of δ_2/D_* versus the Richardson number $\widehat{Ri}_l$.

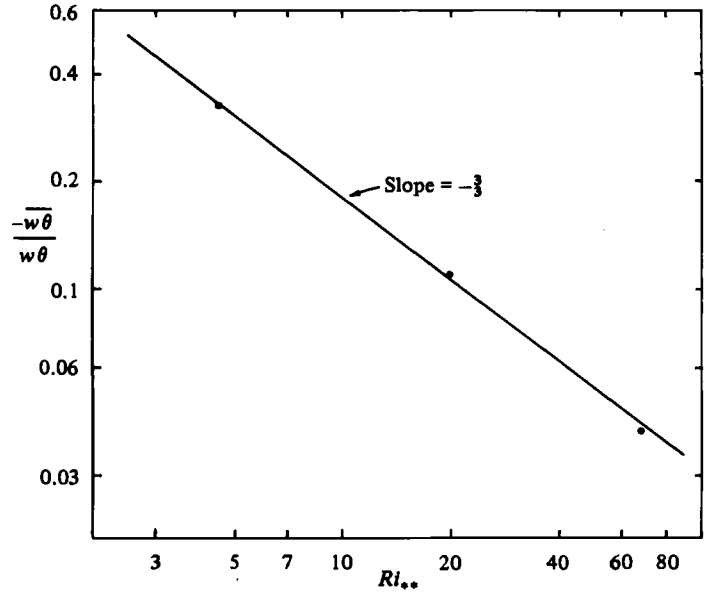

FIGURE 20. Variation of $-\overline{w\theta}/w\theta$ with the Richardson number $Ri_{**} = g\Delta T\delta/Tu_*^2$ in the interfacial layer (from Piat & Hopfinger 1982).

flux is the only available energy source at the entrainment interface. Figure 20 shows the variation of $I \propto (-\overline{w\theta}/w\theta)$ (θ is the temperature fluctuation) versus Ri_{**} ($= g\Delta T\delta/Tu_*^2$) at the entrainment interface as extracted from figure 11 of Piat & Hopfinger (1981). In the definition of Ri_{**}, T, ΔT and u_* represent the temperature, temperature jump across the interfacial layer and the friction velocity at the plate, and δ is the boundary-layer thickness. The results show decreasing behaviour of the

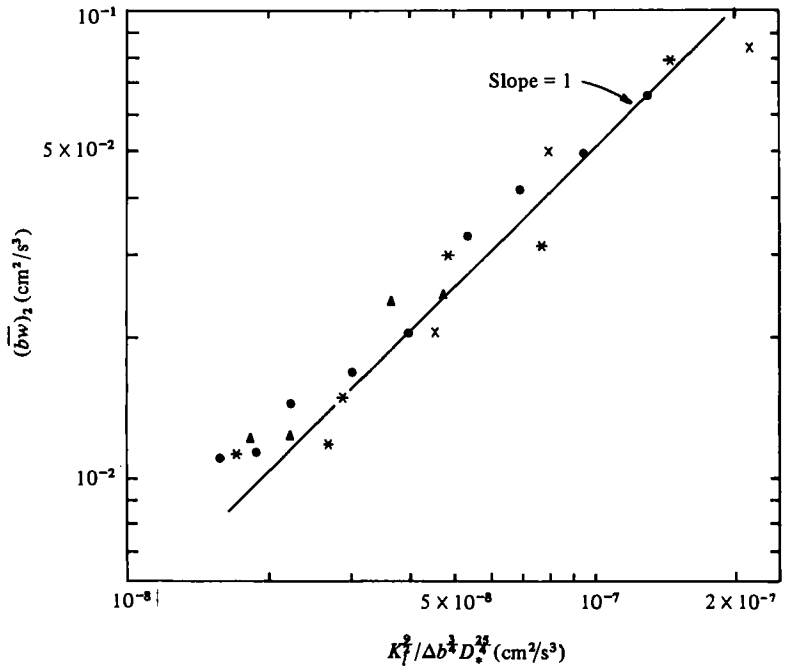

FIGURE 21. A log–log plot of $(\overline{bw})_2$ versus $K_l^2/\Delta b^{\frac{3}{4}} D_*^{\frac{25}{4}}$. Symbols have the same meaning as in figure 9.

intermittency factor with increasing Richardson number and lend some additional support to (55). Thus the ratio $\overline{w\theta}/w\theta$ in a stratified fluid depends strongly on the stability and cannot be assumed to be a constant as conjectured by Townsend (1957).

6.7. *Experimental verification of the closure hypotheses in Long's theory*

As we saw in §4, an important closure assumption in Long's (1978*b*) theory is that the dissipation in the turbulent patches does not depend on stability, but only on the location of the patch in the interfacial layer and on the depth of the mixed layer. The resulting equations (36)–(38) can be combined with the observed relationship $h = \alpha_1 D_*$ to yield

$$q_2 = -\frac{A_3 \alpha_1^{\frac{3}{4}}}{B_7} \frac{K_l^2}{\Delta b^{\frac{3}{4}} D_*^{\frac{25}{4}}}, \tag{56}$$

$$P = \frac{q_2}{2} + \frac{u_e \Delta b}{2\alpha_1} = \frac{A_4 \alpha_1^{\frac{3}{4}}}{B_7} \frac{K_l^2}{\Delta b^{\frac{3}{4}} D_*^{\frac{25}{4}}}, \tag{57}$$

$$Q = u_e \Delta b - q_2 = \frac{6 A_5 \alpha_1^{\frac{7}{4}}}{B_7} \frac{K_l^2}{\Delta b^{\frac{3}{4}} D_*^{\frac{25}{4}}}. \tag{58}$$

Log–log plots of q_2, P, Q versus $K_l^2/\Delta b^{\frac{3}{4}} D_*^{\frac{25}{4}}$ are shown in figures 21–23. These reveal excellent agreement with (56)–(58).† As we have already remarked, the parameters A_3, A_4 and A_5, introduced in Long's (1978*b*) formulation as 'constants' depending on the stability of the non-turbulent layer, can be treated as universal constants in the present problem.

† The excellence of the agreement in figures 21–23 with the closure conditions (56)–(58) is not surprising in view of the excellence of the agreement of the data of Fernando & Long (1983) with the prediction of Long that h/D_* is constant and that $u_e D_*/K$ is proportional to $Ri^{-\frac{7}{4}}$, because these imply (56)–(58).

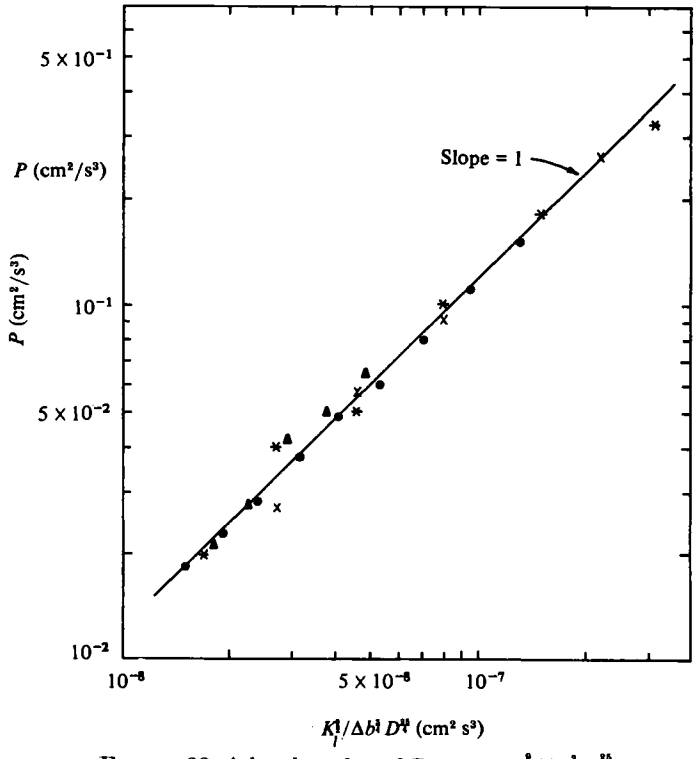

FIGURE 22. A log–log plot of P versus $K_l^3/\Delta b^3 D_*^{\frac{1}{2}}$. Symbols have the same meaning as in figure 9.

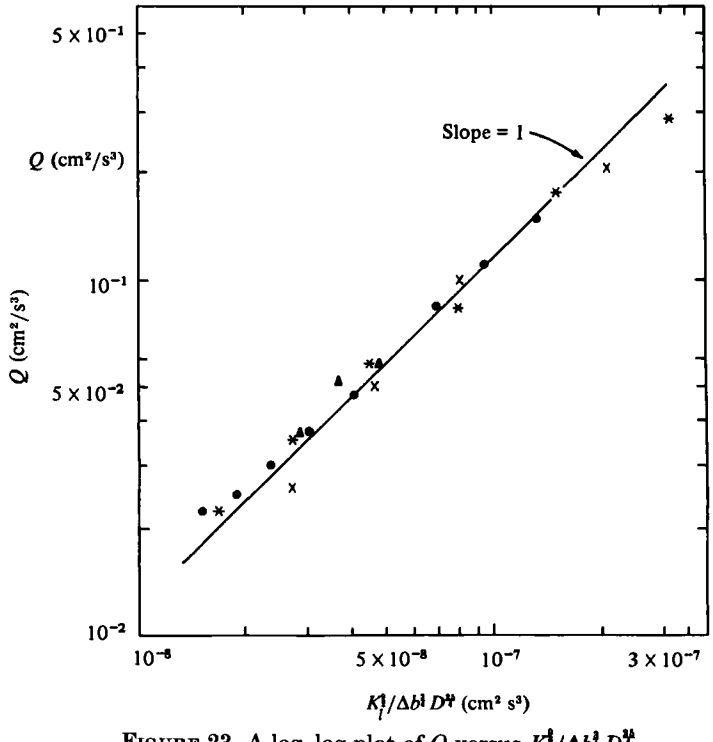

FIGURE 23. A log–log plot of Q versus $K_l^3/\Delta b^3 D_*^{\frac{1}{2}}$. Symbols have the same meaning as in figure 9.

7. Evaluation of the universal constants in Long's theory

In view of the excellent agreement between the present experimental results and the theoretical predictions of Long (1978*b*), we find it worthwhile to evaluate the various universal constants appearing in §4, especially because some of these numerical values may be generally applicable to stratified-fluid turbulence. For completeness, B_8 and α_2 values from Fernando & Long (1983) have been added:

$$D_* = B_8 V_0^{-\frac{7}{11}} K_l^{\frac{8}{11}} t^{\frac{4}{11}}, \quad B_8 \approx 12.5, \tag{59}$$

$$h = \alpha_1 D_*, \quad \Delta b\, D_*(2+\alpha_1) = 2V_0^2, \quad \alpha_1 \approx 0.22, \tag{60}$$

$$\frac{u_e D_*}{K_l} = \alpha_2 Ri_l^{-\frac{7}{4}}, \quad \alpha_2 \approx 2.64 \times 10^5, \tag{61}$$

$$\frac{w_2 D_*}{K_l} = \alpha_4 Ri_l^{-\frac{1}{4}}, \quad \alpha_4 \approx 38.7, \tag{62}$$

$$\frac{\delta_2}{D_*} = \alpha_5 Ri_l^{-\frac{3}{4}}, \quad \alpha_5 \approx 27.3, \tag{63}$$

$$q_3 = -B_1 u_3 b_3 I_3, \quad B_1 \approx 0.3, \tag{64}$$

$$\epsilon_3 = \frac{B_4 I_3 u_3^3}{\delta_3}, \quad B_4 \approx 0.4, \tag{65}$$

$$I_{23} = \alpha_6 Ri_l^{-\frac{3}{4}}, \quad \alpha_6 = 183.3, \tag{66}$$

$$u_3^2 = B_2 \delta_3 b_3 = B_3 \delta_3^2 \frac{\Delta b}{h}, \quad B_2 \approx B_3 \approx 0.44, \tag{67}$$

$$\frac{w_2^3}{\delta_2} \frac{D_*^4}{K_l^3} = B_6, \quad B_6 \approx 2127, \tag{68}$$

$$\frac{\partial u_3^3}{\partial \zeta} = B_7 q_3, \quad B_7 = \frac{1}{A_2} \approx 1.86 \tag{69}$$

and

$$u_3^3 = \left(\frac{h}{\Delta b}\right)^{\frac{3}{4}} \frac{K_l^2}{D_*^6}\left[B_6^{\frac{3}{6}} B_3^{-\frac{3}{4}} - A_3\left(\frac{\zeta}{D_*}\right) + A_4\left(\frac{\zeta^2}{D_*^2}\right) + A_5\left(\frac{\zeta^3}{D_*^3}\right)\right], \tag{70}$$

where

$$A_3 \approx 2.70 \times 10^6, \quad A_4 \approx 7.29 \times 10^6, \quad A_5 \approx 5.28 \times 10^6. \tag{71, 72, 73}$$

In the above list, B_8, α_1, α_2, A_3, A_4 and A_5 were measured directly. In estimating A_2 and B_7 we used results of the buoyancy-flux measurements, the dissipation estimates with $A \approx 0.61$ in (5) and $r = 0.81$ in (7). α_4/α_5 was measured from the interfacial-layer wave-frequency measurements (§6.5). The result $\alpha_4/\alpha_5 = (B_3/\alpha_1)^{\frac{1}{2}}$ obtained from (43) and (44) was used to evaluate B_3. Note that our value of $B_3 \approx 0.44$ compares very well with the estimate 0.46 of Liu (1982), who measured the turbulent kinetic energy and the potential energy of the eddies when a grid is towed horizontally in a linearly stratified fluid. Once α_2, A_2, α_1 and B_3 are known, B_6 can be calculated from (42). B_3, B_6 and α_1 thus obtained were used to evaluate α_4 and α_5. The value of α_5 was checked by independent measurements of wave amplitude as shown in figure 19. The line drawn corresponds to the indirectly calculated α_5 value. Finally, in taking $B_1 \approx 0.3$ we have used the results of Arya (1975).

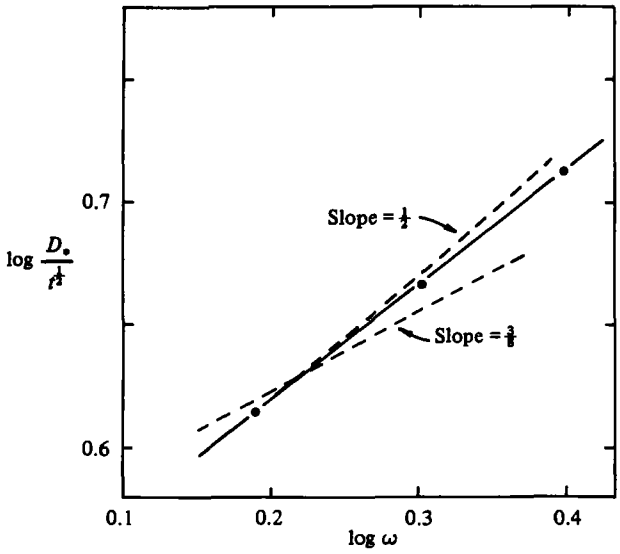

FIGURE 24. A graph of $\log(D_*/t^{\frac{1}{2}})$ versus $\log\omega$.

8. Mixed-layer growth at small Richardson numbers

The involvement of large-scale eddies in the entrainment process at low Ri means that the mixing mechanism in a weakly stratified fluid differs from that in a strongly stratified one. In this section we discuss the mixed-layer growth mechanism at low Richardson numbers.

8.1. *Homogeneous fluids*

The mechanism of entrainment in a homogeneous fluid subjected to zero-mean-shear turbulence is, at present, an open question. According to Corrsin & Kistler (1955), the rate of advance of a turbulent front u_{eK} is determined by the balance between the viscous diffusion of vorticity and the mean-square rate of stretching of vortex lines by the turbulence, i.e. by Kolmogorov's velocity scale $u_K = (\nu\epsilon)^{\frac{1}{4}}$. On the other hand, it is also possible to argue that entrainment is accomplished by the engulfment of the irrotational fluid by the large-scale eddies and the subsequent digestion by the small-scale eddies (e.g. Roshko 1976). In the latter case the deepening rate u_{el} should be proportional to the r.m.s. velocity of turbulence near the interface or $u_{el} \sim \sigma_u$. For oscillating-grid turbulence, $\epsilon = A\sigma_u^3/l$ and $\sigma_u \sim K_l/D_*$, we may write the deepening rates as

$$D_* \sim (K_l^3\nu)^{\frac{1}{8}} t^{\frac{1}{8}} \tag{74}$$

if the viscous diffusion of vorticity is important for the mixed-layer spreading, and

$$D_* \sim (K_l t)^{\frac{1}{2}} \tag{75}$$

if the entrainment occurs by large-scale eddies. Notice that both hypotheses give rise to a $t^{\frac{1}{2}}$ law as observed by Dickinson & Long (1983), and, since $u_{el}/u_{eK} \sim Re_l^{\frac{1}{4}}$, where $Re_l = K_l/\nu$, the two velocities u_{el} and u_{eK} do not differ much in laboratory conditions. However, using the observed relationship $K_l \propto \omega$, we may compare the validities of (74) and (75) by comparing the predicted variations with ω. Figure 24 shows a plot of $\log(D_*/t^{\frac{1}{2}})$ versus $\log\omega$ for the propagation of a front in a homogeneous fluid, using

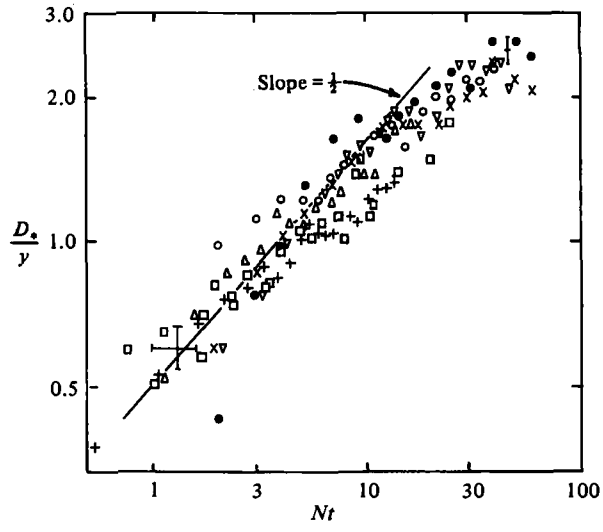

FIGURE 25. A log–log plot of D_*/y versus Nt. The symbols have the same meaning as in Thorpe (1982).

the measurements of Dickinson (1980). Results show closer agreement with (75) than (74), indicating that the propagation of a front created by an oscillating grid in a homogeneous fluid is governed by the action of the large-scale eddies.

8.2. *Linearly stratified fluids*

When a linearly stratified fluid of buoyancy frequency N is agitated by an oscillating grid, the growth of the mixed layer passes through different regimes. Near the grid, the turbulence is so intense (low Richardson number) that the effects of stratification can be neglected, and so the mixed layer propagates as $D_* = (Kt)^{\frac{1}{2}}$, which implies that the large-scale eddies are involved in the entrainment. Normalizing the depth of the mixed layer with $y = S^{\frac{3}{4}}M^{\frac{1}{4}}(\omega/N)^{\frac{1}{2}}$ and using $K \approx 7K_l$, where $K_l = C_2\beta M^{\frac{1}{4}}S^{\frac{3}{4}}\omega$ from (3) and (4), we get

$$\frac{D_*}{y} = (7C_2\beta)^{\frac{1}{2}}(Nt)^{\frac{1}{2}}. \tag{76}$$

This expression may be compared with the experiments of Thorpe (1982), who measured the time evolution of the fully turbulent region of thickness D_*, when a linearly stratified fluid is subjected to the turbulence induced by a vertical grid oscillating horizontally. Figure 25 shows his data in a log–log plot of D_*/y versus Nt. Note that, up to about $Nt \sim 3$, the growth can be well represented by $D_*/y \sim (Nt)^{\frac{1}{2}}$ (indicating independence of N) as in (76), but at large times (or large Richardson numbers) the stratification becomes important and the growth is retarded. The above results are also consistent with the observations of Dickey & Mellor (1980) that the stratification becomes important at times $Nt \sim 2$–3 when a grid is dropped through a linearly stratified fluid.

8.3. *Two-fluid systems at small Ri*

Experiments were performed to investigate the mixed-layer deepening in a two-layer fluid at small Richardson numbers. The grid was placed inside the freshwater layer and the initial density jump was kept very small. Observations indicate that the

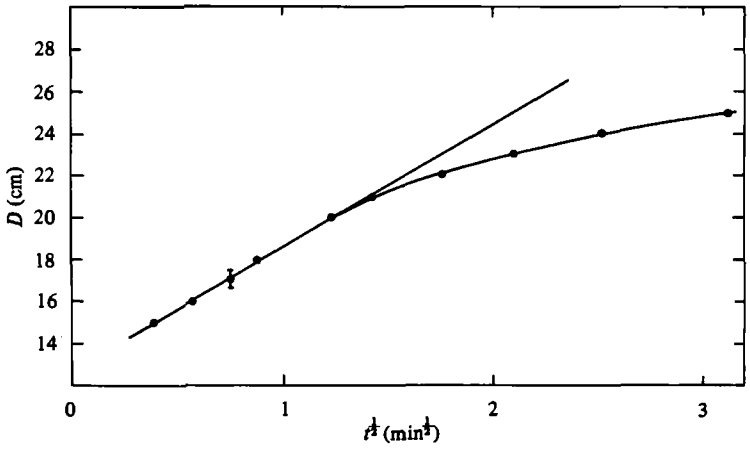

FIGURE 26. A plot of D versus $t^{\frac{1}{2}}$ for a low-Richardson-number experiment ($V_0 = 8.11$ cm/s, $K = 13.64$ cm^2/s).

turbulent front propagates initially as $D_* = (Kt)^{\frac{1}{2}}$, as in a homogeneous fluid. Once the front reaches the density interface, the deepening rate drastically decreases owing to the damping influence on the turbulence of the density differences. As we have mentioned, visual observations indicate that the mixing mechanism involves scouring and splashing by the large eddies. The deepening rate seems to follow a $D_* = \alpha t^{\frac{1}{2}}$ type law to begin with (e.g. see figure 26), but for this regime it is apparent from experiments that α depends on V_0 and K. At large times the deepening law tends to follow $D_* \sim V_0^{-\frac{7}{11}} K^{\frac{2}{11}} t^{\frac{2}{11}}$, and, of course, in this regime small-scale quasi-isotropic eddies are responsible for entrainment and the large-scale eddies tend to flatten against the interface.

We may assume that the large-scale eddies tend to flatten when the buoyancy forces acting on them are of the same order as the inertial forces, i.e.

$$\sigma_u^2 = \gamma_1 l \Delta b, \tag{77}$$

where l is the integral scale near the interface and γ_1 is a constant. Using $l = \beta D_*$, we may write

$$\frac{\sigma_u^2}{\gamma_1 \beta D_*} = \Delta b, \quad \text{or} \quad \sigma_u^2 = \gamma_1 \beta D_* \Delta b \approx \gamma_1 \beta V_0^2, \tag{78, 79}$$

where we use (77) and (4) together with (14). Notice that the expression (79) provides a new physical meaning for V_0. When $\sigma_u \gg V_0$ large-scale eddies do not flatten at the density interface and are directly involved in the entrainment process, whereas when $\sigma_u \ll V_0$ the large-scale eddies tend to flatten. In the present case $\sigma_u \approx K_l/\beta D_*$, and the depth D_{*f} of the mixed layer at which the large-scale eddies tend to flatten is given by

$$D_{*f} \approx (\gamma_1 \beta^3)^{-\frac{1}{2}} K_l / V_0. \tag{80}$$

D_{*f} may be estimated using depth/time records of the mixed-layer deepening if we assume that the transition from $t^{\frac{1}{2}}$ behaviour to the $t^{\frac{2}{11}}$ behaviour occurs when the large-scale eddies tend to flatten and the quasi-isotropic eddies take over the entrainment (Long 1978*b*). A plot of D_* versus K_l/V_0 is shown in figure 27. The best-fit curve to the data points through the origin, has a slope ≈ 42. Taking $\beta \approx 0.25$ we

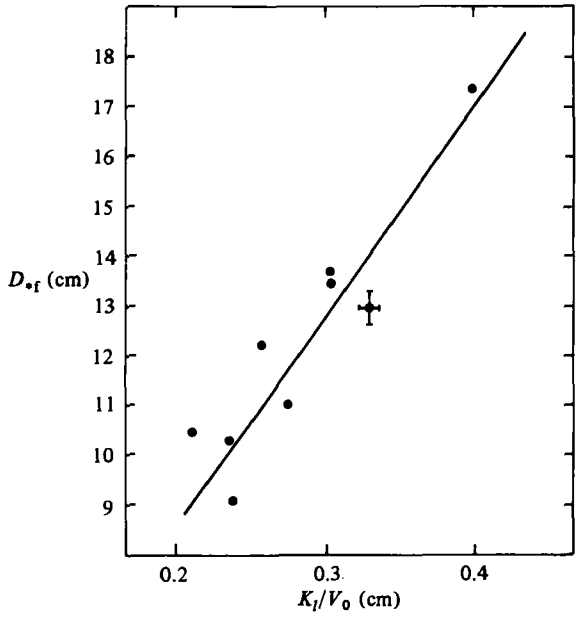

FIGURE 27. Variation of D_{*f} with $L_*(= K_l/V_0)$ for low-Richardson number experiments.

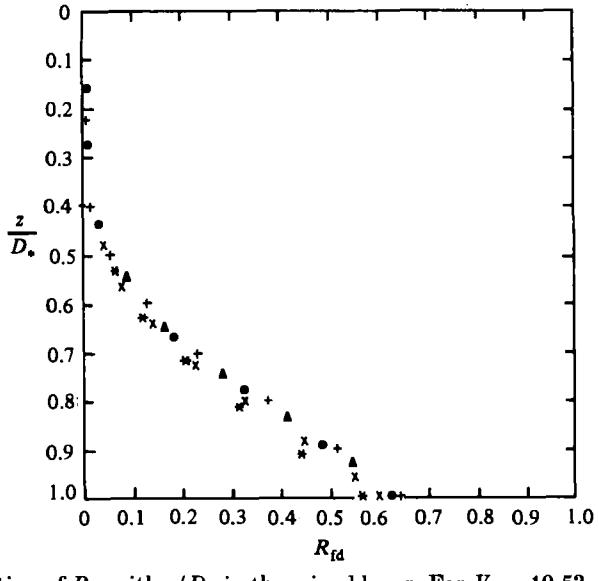

FIGURE 28. Variation of R_{fd} with z/D_* in the mixed layer. For $V_0 = 19.53$, $K = 18.81$ experiment: ▲, $D_* = 21.6$. For $V_0 = 25.80$, $K = 18.95$ experiment: ●, $D_* = 18$; +, 20; *, 22; ×, 24. (D_* in cm, V_0 in cm/s, K in cm²/s.)

estimate $\gamma_1 \approx 0.035$. Accordingly, the large-scale eddies tend to flatten when $\widehat{Ri}_l \approx 1800$ or $\widehat{Ri} \approx 37$, where $\widehat{Ri} = V_0^2 D_*^2/K^2$ and $\widehat{Ri}_l = V_0^2 D_*^2/K_l^2$. This result may be used in understanding the observed deviation of the Hopfinger & Toly (1976) data from the $\widehat{Ri}^{-\frac{1}{4}}$ behaviour at low $\widehat{Ri}$. In figure 12 of Fernando & Long (1983), it is clearly seen that, when $\widehat{Ri} < 37$, the data of Hopfinger & Toly (1976) tend to deviate from the observed $Ri^{-\frac{1}{4}}$ behaviour at higher Richardson numbers.

9. Properties of the mixed layer

Because of the vigorous turbulent mixing, the buoyancy gradients in the mixed layer are extremely weak (e.g. see (46)) and we were unsuccessful in measuring them with the conductivity gauge. However, direct measurements of buoyancy gradients in the mixed layer have been made by Wolanski & Brush (1975), and their measurements are not much different from the prediction of (46) (see their figure 8). To get some indication of the buoyancy effects in the mixed layer, we may calculate R_{fd} at various depths z in this layer. The buoyancy flux q at any z may be written as $q = q_2 z/D_*$, and the dissipation and the energy-flux divergence at any z may be evaluated from (5) and (23). Figure 28 shows the variation of R_{fd} with z/D_*. Note that, in the bulk of the mixed layer, the buoyancy flux is negligible but, as the entrainment interface is approached, the buoyancy flux becomes an appreciable part of the energy budget.

10. Discussion and conclusions

The present experimental study is a continuation of the work of Fernando & Long (1983), and deals with fundamental aspects of turbulent entrainment in a two-fluid system. It may be useful here to summarize the major findings of the full experimental study.

(i) The time-law of growth of a grid-generated turbulent mixed layer in a two-fluid system at high Richardson numbers may be written as (Fernando & Long 1983)

$$D_* \sim V_0^{-\frac{7}{11}} K^{\frac{8}{11}} t^{\frac{8}{11}},$$

where the depth of the mixed layer D_* and the time t are measured from a virtual source plane, whereas in the low-Richardson-number limit mixed-layer growth follows the law

$$D_* \sim (Kt)^{\frac{1}{2}}.$$

The latter excludes the possibility of the involvement of molecular effects in the grid-induced turbulent entrainment in a homogeneous fluid, and lends support for the concept of entrainment by large-scale eddies. The Richardson number Ri_l where the large-scale turbulent eddies are flattened is estimated as about 1800.

(ii) As entrainment proceeds, the initial two-layer system tends to develop a third layer, namely the interfacial layer, within which the buoyancy gradient is constant. The thickness of the interfacial layer grows proportionately to the depth of the mixed layer, and the ratio h/D_* is independent of the Richardson number.

(iii) At high Richardson numbers the entrainment law takes the form $E \propto Ri^{-\frac{3}{4}}$, where E is the entrainment coefficient. The observed deviation of the Hopfinger & Toly (1976) results from the above law at low Richardson numbers (Fernando & Long 1983) may be due to the involvement of large-scale eddies in the entrainment process.

(iv) The buoyancy flux and the dissipation in the mixed layer near the entrainment interface are of the same order, and hence the diffusive-flux Richardson number in this region tends to be a constant. Also, in the bulk of the mixed layer the diffusive-flux Richardson number is negligible, but as the interfacial layer is approached it increases rapidly.

(v) At low and moderate Richardson numbers molecular-diffusive fluxes are negligible.

(vi) Intermittency and the amplitude of the internal waves in the interfacial layer

decrease with the Richardson number, whereas the wave frequency increases with the Richardson number.

(vii) The experimental results show an excellent agreement with a theory due to Long (1978*b*), and the closure assumptions of this theory are also experimentally verified. The universal constants appearing in Long's theory are evaluated.

(viii) After a certain mixed-layer depth the experimental results deviate from Long's (1978*b*) theory, and it was shown in a preceding paper (Fernando & Long 1983) that this may be due to a wall effect.

The authors wish to thank Professors O. M. Phillips, S. A. Kitaigorodskii and Stanley Corrsin for their useful comments, suggestions and discussions during the period of this study, Messrs Ed Bennett and Siniti Oneda for their support in carrying out the experiments, and Ms Kate Francis for typing the manuscript. The authors also wish to acknowledge financial support of the National Science Foundation (Grants ATM-7907026 and ATM-8210498) and the Office of Naval Research (Fluid Dynamics Division, Contract N 0014-76-C-0184). During the period of revision of the manuscript the first author was supported by the National Science Foundation (Grant CEE-7272A1) through the California Institute of Technology.

REFERENCES

Arya, S. P. S. 1975 Buoyancy effects in a horizontal flat-plate boundary layer. *J. Fluid Mech.* **68**, 321.

Batchelor, G. K. 1953 *Theory of Homogeneous Turbulence.* Cambridge University Press.

Bouvard, M. & Dumas, H. 1967 Application de la méthode du fil chaud à la mesure de la turbulence dans l'eau. *Houille Blanche* **22**, 257.

Corrsin, S. & Kistler, A. L. 1955 Free stream boundaries of turbulent flow. *NACA Tech. Note* 3133.

Crapper, P. F. & Linden, P. F. 1974 The structure of turbulent density interfaces. *J. Fluid Mech.* **65**, 45.

Deardorff, J. W., Willis, G. E. & Stockton, B. H. 1980 Laboratory studies of entrainment zone of a convective mixed layer. *J. Fluid Mech.* **100**, 41.

Dickey, T. D. & Mellor, G. L. 1980 Decaying turbulence in neutral and stratified fluids. *J. Fluid Mech.* **99**, 13.

Dickinson, S. C. 1980 Oscillating grid turbulence including effects of rotation. Ph.D. thesis, The Johns Hopkins University.

Dickinson, S. C. & Long, R. R. 1978 Laboratory study of the growth of a turbulent layer of fluid *Phys. Fluids* **21**, 1698.

Dickinson, S. C. & Long, R. R. 1983 Oscillating-grid turbulence including effects of rotation. *J. Fluid Mech.* **126**, 315.

Dillon, T. M. & Powell, T. M. 1979 Observations of a surface mixed layer. *Deep-Sea Res.* **26A**, 915.

Fernando, H. J. S. 1983 Studies on turbulent mixing in stably stratified fluids. Ph.D. thesis, The Johns Hopkins University.

Fernando, H. J. S. & Long, R. R. 1983 The growth of a grid-generated turbulent mixed layer in a two-fluid system. *J. Fluid Mech.* **133**, 377.

Fisher, H., List, J., Koh, R., Imberger, J. & Brooks, N. 1979 *Mixing in Inland and Coastal Waters.* Academic.

Folse, R. F., Cox, T. P. & Schexnayder, K. R. 1981 Measurements of the growth of a turbulently mixed layer in a linearly stratified fluid. *Phys. Fluids* **24**, 396.

Grant, H. L., Moilliet, A. & Vogel, W. M. 1968 Some observations of the occurrence of turbulence in and above the thermocline. *J. Fluid Mech.* **34**, 443.

HINZE, J. O. 1975 *Turbulence*, 2nd edn. McGraw-Hill.

HOPFINGER, E. J. & LINDEN, P. F. 1982 Formation of thermoclines in zero-mean-shear turbulence subjected to a stabilizing buoyancy flux. *J. Fluid Mech.* **114**, 157.

HOPFINGER, E. J. & TOLY, J.-A. 1976 Spatially decaying turbulence and its relation to mixing across density interfaces. *J. Fluid Mech.* **78**, 155.

LINDEN, P. F. 1979 Mixing in stratified fluids. *Geophys. Astrophys. Fluid Dyn.* **13**, 3.

LINDEN, P. F. 1980 Mixing across a density interface produced by grid turbulence. *J. Fluid Mech.* **100**, 691.

LIU, H.-T. 1982 Grid-generated turbulence in a stably stratified fluid. *Fluid Res. Rep.* 224, *Flow Ind. Inc., Washington.*

LONG, R. R. 1970 A theory of turbulence in stratified fluids. *J. Fluid Mech.* **42**, 349.

LONG, R. R. 1978*a* Theory of turbulence in a homogeneous fluid induced by an oscillating grid. *Phys. Fluids* **21**, 1887.

LONG, R. R. 1978*b* A theory of mixing in a stably stratified fluid. *J. Fluid Mech.* **84**, 113.

MCDOUGALL, T. J. 1979 Measurements of turbulence in a zero-mean-shear mixed layer. *J. Fluid Mech.* **94**, 409.

MCEWAN, A. D. 1983 Internal mixing in stratified fluids. *J. Fluid Mech.* **128**, 59.

MOORE, M. J. & LONG, R. R. 1971 An experimental investigation of turbulent stratified shearing flow. *J. Fluid Mech.* **49**, 635.

OZMIDOV, R. V. 1965 On the turbulent exchange in a stably stratified ocean. *Izv. Atmos. Ocean Phys.* **1**, 853.

PHILLIPS, O. M. 1955 The irrotational motion outside a free turbulent boundary. *Proc. Camb. Phil. Soc.* **51**, 220.

PHILLIPS, O. M. 1977 *Dynamics of the Upper Ocean*, 2nd edn. Cambridge University Press.

PIAT, J. F. & HOPFINGER, E. J. 1981 A boundary layer topped by a density interface. *J. Fluid Mech.* **113**, 411.

PRICE, J. F. 1979 Observations of a rain-formed mixed layer. *J. Phys. Oceanogr.* **9**, 643.

ROSHKO, A. 1976 Structure of turbulent shear flows: a new look. *AIAA J.* **14**, 1349.

ROUSE, H. & DODU, J. 1955 Turbulent diffusion across a density discontinuity. *Houille Blanche* **10**, 522.

THOMPSON, S. M. & TURNER, J. S. 1975 Mixing across an interface due to turbulence generated by an oscillating grid. *J. Fluid Mech.* **67**, 349.

THORPE, S. A. 1977 Turbulence and mixing in a Scottish loch. *Proc. Camb. Phil. Soc.* **286**, A 1334.

THORPE, S. A. 1982 On the layers produced by rapidly oscillating a vertical grid in a uniformly stratified fluid. *J. Fluid Mech.* **124**, 391.

TOWNSEND, A. A. 1957 Turbulent flow in a stably stratified atmosphere. *J. Fluid Mech.* **3**, 361.

TOWNSEND, A. A. 1976 *The Structure of Turbulent Shear Flow*, 2nd edn. Cambridge University Press.

TURNER, J. S. 1965 The coupled turbulent transports of salt and heat across a sharp density interface. *Int. J. Heat Mass Transfer* **8**, 759.

TURNER, J. S. 1968 The influence of molecular diffusivity on turbulent entrainment across a density interface. *J. Fluid Mech.* **33**, 639.

WYATT, L. R. 1978 The entrainment interface in a stratified fluid. *J. Fluid Mech.* **86**, 293.

WOLANSKI, E. J. & BRUSH, L. M. 1975 Turbulent entrainment across stable density step structures. *Tellus* **27**, 259.